



**HAL**  
open science

# Analyzing Canopy Heterogeneity of the Tropical Forests by Texture Analysis of Very-High Resolution Images - A Case Study in the Western Ghats of India

Pierre Ploton

► **To cite this version:**

Pierre Ploton. Analyzing Canopy Heterogeneity of the Tropical Forests by Texture Analysis of Very-High Resolution Images - A Case Study in the Western Ghats of India. Head of Ecology Department; Institut Français de Pondichéry; e-mail: ifpeco@ifpindia.org. Institut Français de Pondichéry, 71 p., 2010, Pondy Papers in Ecology no. 10. hal-00509952

**HAL Id: hal-00509952**

**<https://hal.science/hal-00509952>**

Submitted on 17 Aug 2010

**HAL** is a multi-disciplinary open access archive for the deposit and dissemination of scientific research documents, whether they are published or not. The documents may come from teaching and research institutions in France or abroad, or from public or private research centers.

L'archive ouverte pluridisciplinaire **HAL**, est destinée au dépôt et à la diffusion de documents scientifiques de niveau recherche, publiés ou non, émanant des établissements d'enseignement et de recherche français ou étrangers, des laboratoires publics ou privés.

# PONDY PAPERS IN ECOLOGY

ANALYZING CANOPY HETEROGENEITY OF THE  
TROPICAL FORESTS BY TEXTURE ANALYSIS OF VERY  
HIGH RESOLUTION IMAGES – A CASE STUDY IN THE  
WESTERN GHATS OF INDIA.

Pierre Ploton



PONDY PAPERS IN ECOLOGY No. 10

**Analyzing Canopy Heterogeneity of the Tropical Forests  
By Texture Analysis of Very-High Resolution Images -  
A Case Study in the Western Ghats of India**

*Pierre Ploton*

INSTITUT FRANÇAIS DE PONDICHÉRY

The Institut français de Pondichéry (IFP) or French Institute of Pondicherry, is a financially autonomous research institution under the dual tutelage of the French Ministry of Foreign and European Affairs (MAEE) and the French National Centre for Scientific Research (CNRS). It was established in 1955 under the terms agreed to in the Treaty of Cession between the Indian and French governments. It has three basic missions: research, expertise and training in human and social sciences and ecology in South and South-East Asia. More specifically, its domains of interest include Indian cultural knowledge and heritage (Sanskrit language and literature, history of religions, Tamil studies, ..), contemporary social dynamics (in the areas of health, economics and environment) and the natural ecosystems of South India (sustainable management of biodiversity).

*French Institute of Pondicherry*, UMIFRE 21 CNRS-MAEE, 11, St. Louis Street, P.B. 33, Pondicherry 605001, INDIA

Tel: 91-413-2334168; Fax: 91-413-2339534

Email: [ifpdir@ifpindia.org](mailto:ifpdir@ifpindia.org)

Website: <http://www.ifpindia.org>

#### **Author**

Pierre Ploton is from the French Institute of Pondicherry, UMIFRE 21 CNRS-MAE, 11, Saint Louis Street, Pondicherry 605001.

<p>This paper was submitted by the author as an M. Sc. thesis n° AV2010-25 FEM 80436 at Wageningen University (The Netherlands) and Ecole Supérieure d'Agriculture d'Angers (France), under supervision of Dr. R. Péliissier (French Institute of Pondicherry), Dr. J. den Ouden and Dr. J. Clevers (Wageningen University).</p>
--

# Table of Content

<b>List of tables and figures</b>	<b>3</b>
<b>Summary</b>	<b>6</b>
<b>1. Introduction</b>	<b>8</b>
1.1. Context	8
1.2. Background	9
1.3. Strategy	10
1.3.1. Image texture and FOTO framework	10
1.3.2. Tree shade and topography	11
1.3.3. Google Earth™: advantages and drawbacks for scientific researches	13
1.4 Objectives and research questions	15
<b>2. Materials and Method</b>	<b>16</b>
2.1. Materials	16
2.1.1. Study site	16
2.1.2. Satellite data	16
2.1.3. Topographical data	17
2.1.4. Simulated forest scenes	19
2.1.5. Ground control data	20
2.2. FOTO method	22
2.2.1. Overview	22
2.2.2. 2D Fourier Transform and r-spectra	22
2.2.3. Textural ordination based on r-spectra	24
2.2.4. Windows r-spectra characterization	24
2.2.5. Image texture – forest structure relationships and mapping	25
2.3. Google Earth vs IKONOS images	25
2.4. Investigation of topography effect	26
<b>3. Results</b>	<b>27</b>
3.1. Textural analysis	27
3.2. Google Earth-derived textural gradient	31
3.3. Effect of topography	34
3.3.1. Local effect	34
3.3.2. Global effect	35
3.4. Predicting stand structure parameters	40
3.4.1. Plots structure	40
3.4.2. Model calibration	42
3.4.3. Model inversion	46
<b>4. Discussion</b>	<b>48</b>
4.1. Google Earth™ images performances	48
4.1.1. Set up and limits	48
4.1.2. Textural gradients	48
4.1.3. Interest and remarks	51
4.2. Relief variations	51
4.2.1. Contribution to windows macro-heterogeneity	52

4.2.2. Influence on canopy textural patterns	52
4.3. Characterization of tropical forest canopy structure	54
4.3.1. Several scales of spatial heterogeneity	54
4.3.2. Ability of FOTO to discriminate forest structure in our case study	55
4.3.3. Interest and remarks	57
<b>Conclusion</b>	<b>59</b>
<b>Bibliography</b>	<b>60</b>
<b>Acknowledgements</b>	<b>64</b>

## List of tables and figures

### Tables

- Table 1. FOTO explanatory power regarding forest attributes and derived estimates (from Couteron *et al.*, 2005; Proisy *et al.*, 2007)
- Table 2. Class break used to extract aspect and data from the TIN (breaks in degrees).
- Table 3. Morphological parameters of the DART scenes dominant strata (density per stand ( $2.25 \text{ ha}^{-1}$ ), mean crown diameter, mean tree height, DBH of tree with mean height)
- Table 4. Output of 2D-FT on a one or several satellite images: PCA data table
- Table 5. Linear regressions between scene structure parameters and IKONOS-derived textural indices (model 1: first PCA axis used as predictive variable; model 2: 2 first PCA axes used as predictive variables)
- Table 6. Linear regressions between scene structure parameters and GE-derived textural indices (model 1: first PCA axis used as predictive variable; model 2: 2 firsts PCA axes used as predictive variables)
- Table 7. Influence of elevation mean and SD on window ordination scores (derived from IKONOS and G.E. images).  $R^2$  adj. with significance level (p-value: \*\*\* < 0.1%; \*\* < 1%; . < 10%)
- Table 8. Relationships between PCA axes and spatial variables manually computed (Aspect & Combined data). Windows are divided among 3 groups (1: face away to the sun, 2: else, 3: face the sun) and multiple mean comparison tests are carried out (Kruskal & Wallis:  $X^2$  value, Tukey: t-value). Significance levels coded as follow: \*\*\* < 0,1%; \*\* < 1% ; \* < 5% ; . < 10%.
- Table 9. Influence of mean hillshade on window ordination scores (derived from IKONOS and G.E. images).  $R^2$  adj. with significance level (p-value: \*\*\* < 0.1%).
- Table 10. Stand structure parameters collected for 7 1-ha ground-truth plots (horizontal distance) close to the Uppangala village (Western Ghats, India).
- Table 11. AGB estimates and CA1 plot scores (see fig X, left)
- Table 12. Structural parameter prediction inferred from the above regressions and based on IKONOS image. Mean and SD values per cluster of canopy texture.

### Figures

- Figure 1. Effect of topography and canopy structural complexity on crown exposure to the sun. On sun-facing slopes, a larger portion of tree crowns is exposed to the sun (d) relatively to slope facing away from it (a), causing the canopy to appear brighter or darker to the sensor. Canopy roughness or complexity leads to heterogeneous tree shades (c) and an increased canopy self-shadowing in comparison with homogeneous canopy (b) (adapted from Kane *et al.*, 2008).
- Figure 2. Effect of solar angle on tree
- Figure 3. Critical position for aspect class breaks
- Figure 4. Examples of DART scenes
- Figure 5. Plot delineation strategy
- Figure 6. IKONOS images of plot F (left) and G (right). Each image is composed of 4 overlapping 125 x 125 m windows as described in fig x.
- Figure 7. General overview of the FOTO method (from Proisy *et al.*, 2007)

- Figure 8. Examples of r-spectra for two images (100x100 pixels): (a) absence of spatial structure, pixel values generated with a Gaussian white noise (WN) with  $\mu=10\sigma$ . (b) Presence of spatial structure generated by the superimposition of a cosine wave (vertical bands) of amplitude  $\beta$ , a linear trend of amplitude  $\beta$  and a WN ( $\sigma=0.1\beta$ ). The full line represents the r-spectra while the dot line stands for the 5% bilateral confidence interval around 1 (expected value in the absence of spatial structure) (from Couteron *et al.*, 2002).
- Figure 9. IKONOS (top) and hillshade (bottom) view of a forested scene with marked topography variations.
- Figure 10. Main PCA results: (up-left) Eigenvalues histogram expressed in percentage of variance explained, only the 10 first values are plotted; (up-right) correlation circle of spatial frequencies with PCA axes, selective spatial frequencies above the 15<sup>th</sup> wavenumbers for visibility; (bottom) first factorial plan with 5 clusters (K-means, Euclidian distances on windows coordinates along the two first PCA axes), solid black circles illustrate clusters barycenter.
- Figure 11. (top) Averaged standardized clusters r-spectra (bottom) Ratio of averaged r-spectra for successive cluster (solid line) and 5% bilateral confidence interval (dot line).
- Figure 12. DART scenes as supplementary individuals in the IKONOS-derived factorial plan.
- Figure 13. DART modeled structural parameters as a function of DART scenes' coordinate along the first PCA axis used as a textural index. Stand numbers label the observations (see Table X). All  $R^2$  values are significant (p-value < 0.001).
- Figure 14. Eigenvalues histogram (expressed in % of variance)
- Figure 15. IKONOS-based windows ordinates as a function of GE-based ones (dotted line: regression line, full line: non-parametric regression on smooth data (locally-weighted polynomial regression))
- Figure 16. Difference trends between GE and IKONOS-based ordinations (dotted line: linear regression line)
- Figure 17. IKONOS and GE view of windows undergoing an important displacement from the GE to the IKONOS-derived PCA first axis: (left) window ordinated as a very coarse grain on GE (PCA1=-8) and as an intermediate grain on IKONOS (PCA1=0); (right) window ordinated as a very fine grain on GE (PCA1=13) and as an intermediate grain on IKONOS (PCA1=2).
- Figure 18. Influence of abrupt slope changes on window texture. (left) Area displaying two steep slopes of opposite aspects and (right) example of window encompassing textural types.
- Figure 19. (a) Position of windows encompassing two types of canopy texture on the IKONOS-derived first factorial plan, (b) standardized R-spectra of this window group (mean) and of window presented in Figure X and (c) examples of such windows displaying different canopy grain.
- Figure 20. Influence of mean elevation on IKONOS 1<sup>st</sup> axis (left) and GE 2<sup>nd</sup> axis (right)
- Figure 21. Influence of Combined data on IKONOS-derived PCA1 (left) and PCA2 (right). Exposition codes divide windows among the ones facing the sun (3), facing away (1) and else (2); only the subset of windows characterized by a slope between 20.4° and 60.4° is considered. Letters (a, b, c) correspond to significant results of Tukey post-hoc tests.
- Figure 22. (top) Regressions of mean hillshade on windows coordinate along PCA1 (right) and PCA2 (left); dotted lines: linear regression, full lines: non-parametric regression on smooth data; (bottom) Initial bins on mean hillshade (K mean clustering on Euclidian distance) and Tukey post-hoc test results.

- Figure 23. (left) Final bins on mean hillshade and Tukey post-hoc test results; (right) Log ratio technique on the 2 first (top) and 2 extreme (bottom) bins; full lines: log ratio, dotted lines: point-wise confidence interval computed from a F-distribution.
- Figure 24. Regression of mean hillshade (left) and mean elevation (right) on window coordinate along PCA1 after partitioned standardization (IKONOS).
- Figure 25. Relative tree density in function of tree crown position (E : emergent, C+ : high canopy, C- : low canopy, U : understory).
- Figure 26. (left) First plan of CA on 6 equal-count dbh bins (only CA1 is used later on the analysis); (right) Distribution of relative frequencies (%) on 5 dbh bins among plots.
- Figure 27. Ground plot position on IKONOS-derived (left) and Google Earth-derived (right) factorial plans (grid mesh = 2)
- Figure 28. Plots P and H standardized r-spectra derived from IKONOS (gray line) and GE (black line).
- Figure 29. Stand structural parameter (see Tab. 10 & 11) as a function of ground plots score on PCA axis 1 (i.e. index of canopy texture) derived from IKONOS. Adjusted coefficient of determination ( $R^2$ ), root mean square error (rmse) in arithmetic units and relative error (s) in percent are presented in bold character when regression p-value < 0.05.
- Figure 30. Stand structural parameter (see Tab. 10 & 11) as a function of ground plots score on PCA axis 1 (i.e. index of canopy texture) derived from Google Earth<sup>TM</sup>. Adjusted coefficient of determination ( $R^2$ ), root mean square error (rmse) in arithmetic units and relative error (s) in percent are presented in bold character when regression p-value < 0.05.
- Figure 31. (left) Project study area, near to Uppangala village (Western Ghats, India) – black dots represent a GPS trace along the trail road crossing the area; (right) same area overlaid by 125 m side square windows with grayscale corresponding to the canopy texture clusters defined previously (see Fig. x-c (plan PCA) and Tab. X), from black (cluster 1, very coarse canopy grain) to light gray (very fine canopy grain). In the top 19 km<sup>2</sup> (i.e. GE image extent), white crosses represent windows particularly marked by relief-induced illumination discrepancies, resulting in a poor canopy characterization.
- Figure 32. Transform histogram of (a) IKONOS and (b) GE pixel values over the top part of the study area. The X axis displays the actual input data values.
- Figure 33. The two scenes on the left display a macro-heterogeneity, with tree shades gradually more pronounced from the bottom-right to the top-left corner. Such scenes seem particularly overestimated by GE. The two scenes on the right display a particular macro-homogeneity with periodic and rather homogeneous tree shades. Such scenes seem particularly underestimated by GE.
- Figure 34. Averaged r-spectra per cluster of canopy texture on (left) wet evergreen forest of the CWG (window size: 125m) and (right) mangrove forests of French Guiana (window size: 100 m; from Proisy *et al.*, 2007).
- Figure 35. (left) Results of biomass allocation model simulations from Enquist and Nklas (2001); (right) regardless of their dbh (“arbitrary units”), the largest / canopy trees visible from the satellite image and characterized by FOTO may contain information relative to size-frequency distribution of all the trees within the stand.

## Summary

**1.** The structural organization of a forest canopy is an important descriptor that may provide spatial information for vegetation mapping and management planning, such as above-ground biomass or carbon stock estimate. In the case of tropical forests, remote sensing-based structure assessments are often hampered by technical difficulties mainly related to high above ground biomass stocks. In this project, we present a powerful method of canopy texture analysis from very-high remotely sensed images and test the potential of the method for studying the wet tropical forests of the Western Ghats region in Southwest India (objective 1). Topography variations influencing image texture, we investigate its impact on the method results and attempt to mitigate it (objective 2). Lastly, high resolution images prices is an important break to remote sensing-based researches while the quality of freely available image provided by Google Earth™ has proven to sufficient to derived textural information, an interesting stake for forest research that is worth being further investigated (objective 3).

**2.** Based on the multivariate ordination of Fourier spectra, the method allowed us to classify canopy images with respect to canopy grain, i.e. a combination of mean size and frequency of tree crowns per sampling window. We defined a canopy textural gradient on 1557 125-m square windows and test its correlation with several forest structural parameters based on 7 1-ha ground plots. The reference canopy textural gradient derived from IKONOS commercial image is compared through descriptive statistics and linear regressions to the Google Earth-derived one to assess the performance of latter freely-accessible image provider. The effect of topography variations are identified with linear regressions using (1) a set of “exposition codes” attributed to each window and computed with respect to the underlying terrain and the sun position, (2) a hillshade model computed with GIS software. A partitioned standardization, previously used with success to mitigate the effect of image acquisition parameters on the method results, is performed to attempt tackling topography influences.

**3.** We shown that IKONOS-derived canopy textural index enable us to discriminate forested scenes according to the dominance of specific ranges of spatial patterns in the image texture and that this ordination highly and reasonably correlate with structural parameters of modeled forested scenes (e.g.  $R^2 = 0.87$  for mean crown diameter,  $R^2 = 0.95$  for mean tree density) and ground plots (e.g.  $R^2 = 0.54$  for mean tree diameter,  $R^2 = 0.63$  for stand basal area and above ground biomass estimate), respectively. Topography variation induced a “local” effect, arising from the presence of pronounced

geomorphologic features within the scene that bias the ordination of relatively few windows, as well as a more “global” effect related to an increase or decrease of trees shade size according to the underlying terrain and having little but significant influence over windows ordination. The performed correction method allowed us to remove the latter un-wanted influence. Google Earth-derived results were consistent regarding the reference commercial image, with a reasonable correlation between the 1st PCA axes derived from the two image types ( $R^2 = 0.48$ ) and similar trends of regression scores with forest structural parameters (e.g.  $R^2 = 0.67$  for mean tree diameter,  $R^2 = 0.50$  for stand basal area and  $R^2 = 0.51$  for above ground biomass estimate) although the poor model calibration led to unrealistic prediction values on one part of the textural gradient.

**4.** This study investigates several issues of interest for a large-scale applicability of this novel and promising method and shows its good predictive ability on forest structural parameters that may be supported by current theoretical trends in forest ecology (chronosequences approach, metabolic theory). We underline the spurious effect of several sources of spatial heterogeneity (topography-, canopy complexity-related) on the method results and emphasize the need for a greater field effort that would be valuable for both Western Ghats forests characterization and methodological development (efficiency of the topography correction method, notably).

**Keywords:** Canopy texture, Fourier spectra, high-resolution images, forest structure, topography, Google Earth<sup>TM</sup>, Western Ghats

# 1. Introduction

## 1.1. Context

As one of the countries that ratified the Kyoto Protocol of the United Nations Framework Convention on Climate Change (UNFCCC), India is committed to regularly report on greenhouse gases emissions (mainly CO<sub>2</sub>). Since the UN Climate Change Conferences in Montréal (2005) and Bali (2007), the importance of reducing emissions from deforestation and forest degradation in developing countries (REDD) has grown as one of the major challenges in future climate change policy, including mechanisms to compensate countries for stabilizing/increasing forest carbon stocks (Gibbs *et al.*, 2007). The crucial role of the REDD program in the world climate change mitigation strategy has been later on acknowledged during the 2009 15<sup>th</sup> Conference of the Parties in Copenhagen, although global agreements on the multiple political, financial and technical questions that its implementation would raise have not been reached (Minang and Murphy, 2010). In this context, the Indian Space Research Organization recently launched a National Carbon Project in order to (i) assess carbon pools, fluxes and net balance in Indian terrestrial biospheres, (ii) establish a remote sensing-based spatial database for carbon modeling and periodic stock assessments and in turn (iii) support national communications to UNFCCC. The French Institute of Pondicherry (IFP) accompanies these research efforts with specific programs oriented toward the development of methods to estimate and map biomass of the forests of the Western Ghats, one of the largest tropical forests left in India. One basic requirement conditioning REDD efficiency indeed relies on our technical ability to accurately monitor forest carbon stocks across landscapes. The main carbon pools in forest ecosystems are the living biomass of trees and understorey vegetation along with the dead mass of litter, woody debris and soil organic matter. In the case of tropical forests, the living biomass parts contain most of the ecosystem's carbon; indeed, the dead biomass component is the least important among forest biomes due to rapid turnover rates and higher respiration (Thompson *et al.*, 2009). Besides, the above ground living component is the most directly impacted by deforestation and degradations. Estimating forest aboveground biomass (AGB) is therefore one of the most critical steps in quantifying carbon stocks and fluxes, particularly in tropical countries. For that purpose, traditional methods are based on field measurements and rely on direct (destructive sampling) or indirect (allometric equations, conversion from volume to biomass) AGB estimation techniques. Such approaches are often labor intensive, time consuming, hardly implementable in remote locations and fail to provide AGB spatial estimations over large areas (Lu, 2006). On the other hand, retrieving forest stand structure parameters (e.g. tree density, basal area, canopy height) from remotely sensed data allows overcoming some critical field-based approaches' drawbacks (e.g. access to remote locations, national-wide cover) and has proven to be of great interest (e.g. Houghton *et al.*, 2001; Grace, 2004; Boyd and Danson, 2005). Moreover, getting insights into the structural organization of forest canopies over extensive areas is not only valuable in the framework of forests carbon monitoring, but would also provide spatial information for both ecological research (e.g. plant species distributions; Coutron *et al.*, 2003) and operational management/conservation (e.g. vegetation mapping and management planning; Tuomisto *et al.*, 1995).

## 1.2. Background

### *Broad remote-sensing principles*

A variety of airborne and satellites images have been used to characterize forest resources. The remotely sensed information depicted on these images relies on the same principle regardless of the sensor type: “the interaction of electromagnetic radiation with the target and analysis of the returned signal as recorded by a sensor” (Boyd and Danson, 2005). Sensors can be broadly categorized into optical or RADAR and differ in the origin of the target electromagnetic signature. Optical systems measure reflected solar radiation in the visible and near infrared spectral range ( $0.4$  to  $3 \times 10^{-6}$  m), for one or more discrete wavelengths, while RADAR systems measure backscattered microwave radiation at wavelengths ranging from  $1 \times 10^{-2}$  to  $1 \times 10^2$  m (Boyd and Danson, 2005, Eric *et al.*, 1997). This difference in the physical properties of the radiation types measured by the two systems engenders differences in the information collected by the sensors. Optical sensors are traditionally considered to provide information on foliage amount and its biophysical properties (small wavelengths absorbed and scattered by leaves, needles or branches) while RADAR sensors provide information on woody biomass and stand structure (long microwave wavelengths scattered by branches, trunks and ground) (Boyd and Danson, 2005).

### *Forest resources characterization & Problem definition*

Medium resolution satellites equipped with optical devices have been largely exploited in the past decades to yield stand parameter estimates with a spatial resolution of a dozen to several dozen meters (Couteron *et al.*, 2005), such as LANDSAT (eg. Lu *et al.*, 2004), SPOT (eg. De Wasseige and Defourny, 2002) or MODIS satellite (Baccini *et al.*, 2004). However, the accuracy of these estimates and therefore of the derived carbon stocks and fluxes in tropical forests is still spoilt by uncertainty (e.g. Grace, 2004; Houghton, 2005; Ramankutty *et al.*, 2007). Indeed, one of the main reasons for uncertainty in AGB estimates in tropical forests is that the AGB can easily reach values up to  $500 \text{ t.ha}^{-1}$ , largely above the saturation threshold of  $100$  to  $200 \text{ t.ha}^{-1}$  that limits the use of remote sensing instruments, including RADAR systems such as Synthetic Aperture Radar (SAR), for detecting spatio-temporal AGB variations (Imhoff, 1995; Lucas *et al.*, 2007). Some believe that both optical and RADAR systems are unable to detect the whole gradient of biomass found in much of the world's high biomass forests (Proisy 2007, Kasischke *et al.*, 1997). **Addressing topical forests degradation issues is therefore greatly hindered by this technical difficulty.**

The potential of recent generation of very high resolution (VHR) optical data provided by IKONOS or QUICKBIRD satellites have not been fully explored for tropical forest structure parameter estimations (Proissy *et al.*, 2007 ; Greenberg *et al.*, 2005) although they may deliver a greater thematic accuracy (Mumby and Edwards, 2002). If there has been an emphasis in the scientific community to develop relationships between spectral signals and biomass (Li and Strahler, 1992), traditionally with classification techniques on an individual pixel basis, such approach may be neither relevant (Greenberg *et al.*, 2005) nor always reliable (Leboeuf *et al.*, 2007) with metric and sub-metric optical data. Hay *et al.* (1996) indeed underlined that as the image spatial resolution increases, so does the inter-class spectral variability of surface features, resulting in poorer classification accuracy. Besides, at such spatial resolution, a pixel encompasses a portion of a single object (e.g. branch) rather than an unknown combination of several scene objects. Target objects (e.g. individual tree

crowns) being larger than a pixel, analyses integrating pattern recognition or image segmentation should improve the spectral or textural information used later on to perform classification (Greenberg *et al.*, 2005, 7; Hay *et al.*, 1996; Malhi *et al.*, 2008).

To day, VHR images have mostly been used for visual tree crown delineation in tropical forests (e.g. Asner *et al.*, 2002, ; Read *et al.*, 2003), while few studies have been investigating automatic analysis approaches. Tree crown delineation, both visual and automatic, do not accurately estimate tree crown size distribution so far (Asner *et al.*, 2002), mostly because of the complex geometry of tropical canopies that are often too aggregated or merged so it gets often difficult to differentiate a group of small crowns from a single large one. The gain in detail allowed by VHR data, notably in terms of brightness variations (i.e. contrast between shadowed and illuminated canopy) is potentially informative (Proisy *et al.*, 2007) and **might be exploited using textural analyses.**

### ***1.3. Strategy***

#### ***1.3.1. Image texture and FOTO framework***

Despite its importance in image interpretation, texture is a complex concept that has not been formally defined (Bharati *et al.*, 2004; de Jong and Van der Meer, 2004). The term generally goes along and characterizes image properties such as smoothness, coarseness, symmetry, regularity, etc. and represents tonal or brightness variations within an image or spatial domain (Bharati *et al.*, 2004; de Jong and Van der Meer, 2004). Providing information on arrangements of objects and their spatial relationships within an image, texture has proven to be of primary importance for landcover classification (de Jong and Van der Meer, 2004) and to predict forest attributes (Wulder *et al.*, 1998). Diverse approaches have been developed to analyze texture and they mainly differ by the method used to extract the textural information (Bharati *et al.*, 2004). These approaches can be broadly categorized as statistical, structural or spectral methods (see de Jong and Van der Meer, 2004). In this project, we adopted a spectral approach and more specifically the Fourier Transform Ordination method (FOTO).

FOTO is a novel approach that has been applied on various forest types, with different input data (aerial photographs, satellite images) and for different aims. However, it proved to consistently characterize tropical canopy structure (e.g. Coutron *et al.*, 2005) and at broader scale, semi-arid ecosystem patterns (e.g. Barbier *et al.*, 2006; Coutron *et al.*, 2006).

First applied to the evergreen rain forest of French Guiana, FOTO was used to characterize and predict forest structural attributes from a single digitized aerial photograph (Coutron *et al.*, 2005). This initial attempt led to good models' explanatory powers on several stand attributes (see Table 1) with no sign of saturation on dense locations. With the wish to apply the method over large areas, the logical next step was to test if such promising results would hold true for sub-metric satellite images, which would therefore simplify image handling (geocoding & mosaicing). Proisy *et al.* (2007) used a set of 1-m panchromatic IKONOS images to derive AGB estimate of the mangrove forests of the same country. It is worth stressing that satellite images were used without any radiometric or geometric corrections, except the ones already applied by the image provider. The study confirmed the potential of the method. Indeed, compared to the former study, a similar canopy grain textural range was found and it allowed the method to consistently discriminate mangroves with respect to their development stage. Moreover, FOTO-derived AGB estimates did not show

saturation for biomass values above 400 t.ha<sup>-1</sup> of dry matter as well as any obvious variance increase, while having a reasonable accuracy (Table 1).

Table 1. FOTO explanatory power regarding forest attributes and derived estimates (from Couteron et al., 2005; Proisy et al., 2007)

Forest type	Forest attribute	Field data range	Determination coefficient (R <sup>2</sup> )	RMSE
Evergreen rain forest	Density (tree / ha)	455 - 861	0.80	
	mean diameter (cm)	20.6 - 34.2	0.71	
	Height (m)	21.1 - 30.4	0.57	
Mangrove forest	AGB (t DM.ha <sup>-1</sup> )	80 - 436	0.91	33

Recently, Barbier et al. (2009) used images extracted from Google Earth<sup>TM</sup> to characterize apparent crown size of Amazonian *terra firme* forests using the FOTO method. Despite their interesting findings on forest dynamics over the region, the authors used a set of artificially generated canopy scenes simulated using a light interception model (see: 2.1.4 Simulated forested scenes) to identify and tackle the influence of image acquisition parameters on the FOTO outputs. Indeed, variations in scene acquisition parameters, namely sun and sensor vertical angles and sun-sensor azimuthal angle, do influence size and proportion of tree shadows, and therefore the parameters FOTO characterized.

FOTO has been applied in very few case studies, and many remain to be investigated in order for this method to be validated and fully operational in various circumstances. In this project, our main objective is to assess the performance of the FOTO method in predicting stand structure parameters (including AGB estimate) for the wet evergreen forests of the Western Ghats (India) (**objective 1**).

### ***1.3.2. Tree shade and topography***

One major issue, which could be a serious limit for applying the method in mountainous areas such as in our study site, the Western Ghats, is the potential bias introduced by the study area geomorphologic features on the FOTO results. Indeed, one may logically wonder whether terrain variations, as image acquisition parameters, would have the potential to influence tree shadows and therefore alter our canopy textural analysis. Whilst Couteron et al. (2005) noticed this influence of relief variations on the results, Proisy et al. (2007) and Barbier et al. (2009) focused on areas virtually flat, i.e. mangrove forests and the Amazon basin. This specific issue has not been investigated so far, although identifying and tackling relief influence on FOTO results may be critical for any large scale implementation of the method, particularly in hilly landscapes.

Shadowing is an inherent part of remote sensing-based land-surface studies (Asner and Wamer, 2003) and the relationship between shadow in forested scenes and the structural features of the given forest have been acknowledged for long (e.g. Asner and Wamer, 2003; Kane et al, 2008; Li and Strahler, 1992) even though it is still poorly understood (Kane et al, 2008). Gu and Gillespie (1998) distinguished three scales of interactions between forest and light. The first interaction take place at the leaves – branches – trunk scale (“tree elements”) and is controlled by their biochemical properties and structure, resulting in specific scattering, transmission and absorption of light. The second level takes place at the tree crown scale

where light redistribution within the crown is controlled by its biophysical properties (leaf density, distribution, orientation). The third and coarser scale is at the canopy level where light interactions among tree crowns influence the directional distribution as well as the radiance intensity as observed by the sensor. At this latter scale, tree shade consists of visible shadows or darkening cast by tree or branch on another one (Kan *et al.*, 2008) and/or on the ground (Li and Strahler, 1992) and vary with canopy geometric complexity (see fig 1, b - c). Attributes of tree shade, such as area or length, should be correlated with crown attributes such as dimensions, height or even diameter at breast height (dbh) (Li and Strahler, 1992 ; Oladi, 2001). The tree shade fraction, defined as the sum of individual tree shade areas divided by a reference ground area, has indeed been used in numerous studies to derive forest structural attributes (e.g. Leboeuf *et al.*, 2007). However, topographic variations are known to complexify shade analyses by adding noise to classification processes (Gu and Gillespie, 1998; Kane *et al.*, 2008). Because trees are geotropic (i.e. growing straight up), topography does not influence the two firsts forest-light interaction scales mentioned earlier. The effect of topography is introduced at the third scale, because it does directly influence the relative arrangement of trees (Gu and Gillespie, 1998). It results that the proportion of sun-lighted tree crowns increases as the slope becomes more pro-sun and vice versa, so that the canopy appears brighter or darker to the sensor due to topographic variations (Gu and Gillespie, 1998; Kane *et al.*, 2008; see fig. 1 a - d)

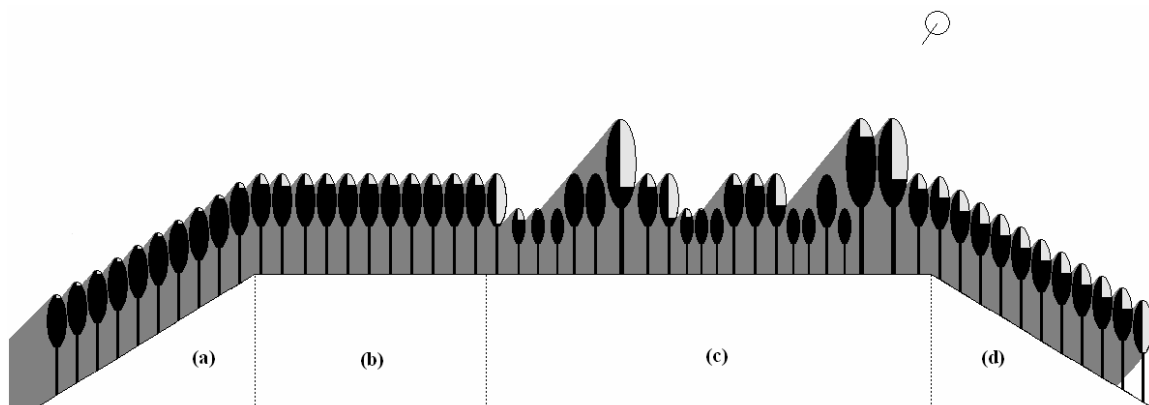


Figure 1. Effect of topography and canopy structural complexity on crown exposure to the sun. On sun-facing slopes, a larger portion of tree crowns is exposed to the sun (d) relatively to slope facing away from it (a), causing the canopy to appear brighter or darker to the sensor. Canopy roughness or complexity leads to heterogeneous tree shades (c) and an increased canopy self-shadowing in comparison with homogeneous canopy (b) (adapted from Kane *et al.*, 2008).

In order to consistently characterize forest canopy texture along the pronounced reliefs of the Western Ghats, it is therefore necessary to normalize our canopy textural gradient to account for the effect of topography variations (**objective 2**).

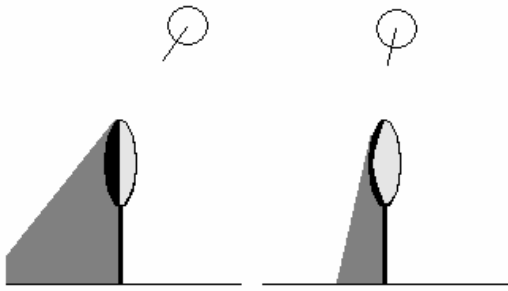


Figure 2. Effect of solar angle on tree shade

This technique has been successfully used to factor out the un-wanted influence of e.g. solar angle on the FOTO-derived canopy textural gradient.

For instance, a low solar angle results in extended, large shadows while a sun position closer to the zenith reduces shadow size as observed by the sensor (Fig. 2). It is therefore necessary to minimize the variability induced by this parameter to consistently characterize canopy scenes acquired with different sun elevation angles. To do so, unit-windows (i.e. sub-part of the satellite images) were split into groups of homogeneous sun elevation angle (considered as a discrete factor) and the FOTO index was standardized per group. This simple technique allowed normalizing the canopy textural gradient regarding this parameter effect. A similar approach may be used to account for the potential influence of topography variations. To apply this technique however, it is necessary to define an index or gradient that would mimic the effect of topography variations on tree shadows and allow gathering unit-windows with homogeneous index values (see 2.1.3 Topographical data).

### ***1.3.3. Google Earth <sup>TM</sup> : advantages and drawbacks for scientific researches***

Another important issue that is worth being investigated is the performance of Google Earth <sup>TM</sup> in providing quality image data for textural analyses. The successful characterization of Amazonian forests apparent crown sizes based on GE images (Barbier et al., 2009) may hold the promise of cost-limited extensive forest resource assessments, a particularly valuable feature in developing countries.

Nowadays, Google Earth <sup>TM</sup> (GE) provides high resolution satellite images that have only recently been used in scientific researches such as to validate MODIS tree cover models (Montesano et al., 2009) or Land Cover maps (Cha and Park, 2007). This newly available tool, largely unexploited by the scientific community (Potere, 2008), comes with advantages and drawbacks that condition its use for scientific purposes.

One serious limitation of commercial VHR images is the expense involved for their acquisition, and that is the main and obvious advantage of the GE archive database since it contains rapidly expanding and cost-free VHR satellite images. In terms of VHR, GE hosts Quickbird and IKONOS images from Digital Globe and Geoeye providers, respectively, while areas where VHR is not available are covered by moderate-resolution sensors such as Landsat (Potere, 2008). Moreover, a vector layer delineates the contour of each satellite image, and basic image metadata are available under the option “More” of the GE “Primary Database”. Together with the name of the image provider and the year of image acquisition that are displayed once the user zooms to a fine detail level, it allows the identification of the image displayed with a reasonable confidence.

A large body of work has been devoted to develop methods and models in order to correct for topographic effect on optical remotely sensed imagery. Traditional methods are based on pixel radiance correction on the raw image, as reviewed by Soenen et al. (2005). However, these correction methods come at the cost of complex algorithms and are known to be heavily time consuming. In this

project, we adopt the standardized partition technique, as described by Barbier et al. (2009).

There is no public documentation detailing the process by which satellite images are added to the GE databases, notably in terms of spectral modification, spatial interpolation (Potere, 2008), or geo-coding. However some ground observations can be made.

Images are orthorectified and projected in a geographic projection system using WGS-84 datum (Potere, 2008), with a narrower spectral range and sometimes a slightly coarser spatial resolution than the underlying commercial image. Indeed, for the spectral component, images are extractable in true color composite (RGB) without the near infrared channel (Potere, 2008, Montesano et al., 2009, Barbier et al., 2009). Concerning the spatial resolution, there is no clear agreement among scientific GE users. For example, GE images overlying Quickbird native images has been referred to has either high resolution images (2.44 m at nadir, e.g. Montesano et al., 2009, Potere, 2008) or very high resolution (0.6-0.7m at nadir) which correspond to the pan-sharpened version of the multispectral high resolution image (e.g. Barbier et al., 2009, Alparone et al., 2007). However, over areas covered by IKONOS images, it seems clear that the spatial resolution is finer than 4 meters per pixel (i.e. the one of IKONOS multispectral images) which could indicate that GE hosts the VHR pan-sharpened products (1-m per pixel), at least in the case of IKONOS native images.

Another critical GE image property that may limit its utility for scientific research is the georegistration quality. Potere (2008) studied the horizontal positional accuracy of GE images over various regions of the world and found an overall accuracy of 39.7 m (0.4 – 171.6m). The more “developed” countries benefited from a significantly better positional accuracy than “developing” countries, with 24.1m and 44.4m of root mean square error (rmse) respectively. For western and south Asia, the positional accuracy was 42.3 m (rmse) and ranged from 1.4 to 115m.

To sum up, if GE images are not the exact replicates of commercial images, they still contain a large part of the information provided by the later, notably in terms of pixel spatial resolution, and therefore can represent an interesting alternative since they are free of cost. For example, methods such as FOTO, with an important need in spatial resolution and which is less relying upon the spectral information component, could particularly value GE data. It would be interesting to compare FOTO outputs with GE images and the underlying commercial satellite image, given the public knowledge hole revolving around GE image integration process, and this is the last objective of this study.

## ***1.4 Objectives and research questions***

**Objective 1:** To assess the performance of the FOTO method in predicting stand structure parameters (including AGB estimate) for the wet evergreen forests of the Western Ghats, India.

- Does the FOTO-derived textural gradient correlate with ground truth sampling plot parameters?

**Objective 2:** To identify and investigate ways to mitigate the potential influence of topographic variations on FOTO results.

- Do topographic variations influence the FOTO-derived canopy textural gradient?

- How could a Global Digital Elevation Model (GDEM) be used to mitigate this influence?

**Objective 3:** To investigate the potential of Google Earth data as input for the FOTO method.

- Does FOTO run over GE images leads to a similar textural gradient as over IKONOS images?

- Does the textural indice(s) derived from G.E. images correlate with ground truth sampling plot parameters?

## 2. Materials and Method

### 2.1. Materials

#### 2.1.1. Study site

The study area is part of the humid forests of the Western Ghats, broadly located within a stretch of 60 to 100 km, south of 15°N latitude along the south-western coast of India. In this area, complex interactions between the relief variations of the Ghats and the summer monsoon rains determine a wide array of forest habitats, from wet evergreen to moist deciduous, more or less degraded formations. Acknowledged for their biological diversity, and particularly their high level of endemism, these forests brought the region to the rank of World Biodiversity Hotspot (Myers et al., 1990).

The project specially focused on an area of about 30 km<sup>2</sup> of wet evergreen forests located on the west-facing escarpment of the Ghats, in the Kadamakal Reserve Forest (Kodagu District, Karnataka), near the Uppangala village. These forests receive an annual rainfall higher than 5 000 mm with a marked dry season between December and March and a rainfall peak in June-July (Pascal and Pélissier, 1996). The general South Indian geology is made up of archaic rocks of the Precambrian shield dominated by gneisses and granites. The Kadamakal reserve soils have been classified as highly desaturated, impoverished ferrallitic soils (Ferry, 1992, in Pascal and Pélissier, 1996) and display two co-habiting facies that dominate according to the local geomorphology : deep alterites on the interfluves and thin, rocky boulders-full soils on the slopes shaping the thalwegs (Pélissier, 1995). If the area has been recently included in the Pushpagiri Wildlife Sanctuary, which consolidate its protection status, it has been partly exploited in the 70-80s by selective logging of less than 10 trees a hectare (unique rotation) (IFP Database) and later on subject to wild fires on certain locations (Madelaine-Antin C., 2009).

This area is of particular interest for this project since its forests' AGB is known to have an upper range of at least 450 t.ha<sup>-1</sup> of dry matter (Flavenot, 2009) and it presents a varied geomorphology responsible for the stand structure to vary accordingly (Pélissier 1995).

#### 2.1.2. Satellite data

The study area has been delineated according to the availability of very high resolution Google Earth<sup>TM</sup> images. The native commercial images are provided by Geoeye<sup>TM</sup> - IKONOS 2<sup>TM</sup> and have been taken in January 2002. Full IKONOS 2 imagery metadata are provided as Appendix 1. GE images are extracted at the image size of 2400 x 2091 pixels from the commercial version of the software. The user view is set to 4.15 km altitude which corresponds to an image spatial resolution of about 2 meters per pixel. GE logos are masked and RGB true color composite bands averaged in a single grayscale layer using ER mapper 7.0 (Earth Resource Mapping Ltd.).

The commercial image used is the GE native image (IKONOS 2<sup>TM</sup>). We used the panchromatic version of the image, which correspond to a wavelength of 0.45–0.93 µm and a spatial resolution of 1 m per pixel. The image was delivered in a georegistered UTM projection encoded in GEOTIF format.

### 2.1.3. Topographical data

The ASTER Global Digital Elevation Model (DEM) released in June 2009<sup>1</sup> and displaying a 30 m spatial resolution was used in GIS software (ArcGis 9.0) to derive several “topographical” variables.

We first utilize the “AnalyseParMailles” ESRI plug-in to create a polygon-shapefile over the DEM data that matched the windowing process of FOTO (see 2.2.1. FOTO Overview). Each polygon was representing one subpart (i.e. unit-window) of the satellite image and overlying the related topographical conditions (DEM data). Three types of variables were then extracted per polygon.

First, we used the Zonal Statistics function of the Spatial Analyst tool (Arctoolbox) to simply extract the mean and standard deviation of the elevation data.

A Triangulated Irregular Network (TIN, Peucker et al., 1978), commonly used to describe surface morphology, was then derived from the DEM with 3D Analyst tool (z tolerance: 5m). A TIN is a vector-based layer that models the surface with a network of non-overlapping triangles built upon a set of points (“nodes”) and satisfying, in this case, the Delaunay triangle criterion. Each triangle facet describes the behavior of the surface (slope, aspect, surface area, etc). We extracted from the TIN model aspect and slope data based on the class breaks described in Table 2.

For the aspect data, class breaks were defined as described in Figure 3. The sun azimuth angle is about 148° on our scene; surfaces that face this direction (toward “1”) are fully illuminated and surfaces facing away to this direction (toward “2”) are shadowed. To characterize these differences in window “exposition” to the sun, we consider 3 sectors on the aspect cycle : (1) face the sun (centered on 148°), (2) face away from the sun (centered on 328°) and (3) else. For (1) and (2), we define 3 sector widths: ±20° ; ±30° and ±40° which correspond to the class breaks 1, 2 and 3 respectively (Tab. 2). These 3 “tolerance” ranges have been subjectively defined by assessing the window subsets characterized as (1) and (2) with varying sector widths and with respect to the visual impression of illumination intensity displayed by each window.

Slope data were divided into 3 classes. The sun elevation angle is about 50° on our scene; we considered that the effect of slope on surface illumination may be maximum when the surface is perpendicularly hit by light rays (i.e. slope = 40°). We therefore build a class around this figure with a subjective ±20° tolerance range (Tab. 2)

Table 2. Class breaks used to extract aspect and slope data from the TIN (breaks in degrees).

	Sector	Break 1	Break 2	Break 3
Aspect	1	128 - 168	118 - 178	108 - 188
	2	308 - 348	298 - 358	288 - 360 0 - 8
	3	0 - 128 168 - 308 348 - 360	0 - 118 178 - 298 358 - 360	8 - 108 188 - 288
Slope	0	0 - 20.4		
	1	20.4 - 60.4		
	0	60.4 - 90		

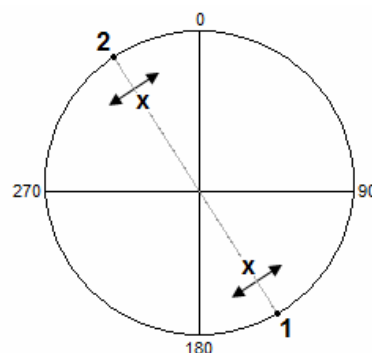


Figure 3. Critical position for aspect class breaks

<sup>1</sup><http://asterweb.jpl.nasa.gov/gdem.asp>

Once computed, slope data were directly combined with aspect data (intersect function, 3D Analyst tool) in order to create triangles characterizing both slope and aspect of the surface (referred to as “combined data”). We only retain the combination with Aspect class break 3 later on this report. This combination allow to further divide the “aspect” window subsets between “optimal slope” (i.e.  $20.4^\circ < x < 60.4^\circ$ ; maximum illumination) and “else” (i.e.  $x < 20.4^\circ$  or  $x > 60.4^\circ$ ) and therefore facilitate trends detection.

The Aspect and Combined data were derived for the whole DEM and afterwards extracted per polygon or unit-window. Each polygon was characterized by either one or more TIN triangles; in the latter case the largest triangle was retained to characterize the given window exposition.

Finally, a hillshade model was created with the DEM data and the light source parameters corresponding to the satellite image metadata. The mean hillshade value per polygon was extracted with the Zonal Statistics function of the Spatial Analyst tool. The hillshade function (3D Analyst) combines slope and aspect data (derived from the DEM) with illumination angle and direction (derived from the light source parameters) and results in a raster layer containing local illumination value per raster cells. Hillshades are commonly used in spatial mapping, notably as “cheap and fast” technique in landslides studies (e.g. Van Den Eeckhaut et al., 2005; Lee and Choi, 2003) because it facilitates topography perception, but also in ecological researches involving spatial variations of solar radiations (e.g. species distribution : Noguchi and Yoshida, 2005; soil moisture index: Iverson et al., 2004). In forest canopy researches, Hillshades have been notably used to quantify the proportion of shadowed canopy and in turn assess e.g. the effectiveness of topography correction methods (Kane et al., 2008) or the canopy light-use efficiency (Hilker et al., 2008).

### 2.1.4. Simulated forest scenes

We used a set of artificially generated canopy scenes that Barbier *et al.* (2009) created using the so-called DART model (Discrete Anisotropic Radiative Transfert, v.2.0.4, CESBIO). This light interception model is able to simulate radiative transfer over potentially complex/heterogeneous 3D scenes in the entire optical domain and to take into account atmospheric radiative transfer and topography variations. Complete description of the model has been published elsewhere (Gastellu-Etcheberry *et al.*, 1996; Gastellu-Etcheberry *et al.*, 2004). The following scenes correspond to two forest strata simulated in the visible domain without atmospheric or topography interactions. Table 3 presents the range of morphological parameters used to model the dominant stratum and Fig. 4 illustrates some of those DART scenes. Refer to Barbier *et al.* (2009) for full details on DART model parameterization.

Table 3. Morphological parameters of the DART scenes dominant strata (density per stand ( $2.25 \text{ ha}^{-1}$ ), mean crown diameter, mean tree height, DBH of tree with mean height)

Stand	Density	crown (m)	height (m)	d.b.h. (m)
1	3	25.00	71.0	1.7
2	36	21.42	60.3	1.4
3	69	18.75	52.4	1.2
4	102	19.75	55.4	1,3
5	135	15.00	41.4	1.0
6	168	12.50	34.1	0.8
7	201	10.71	28.9	
8	234	9.37	25.1	0.6
9	267	8.33	22.2	0.5
10	300	7.50	19.8	0.5

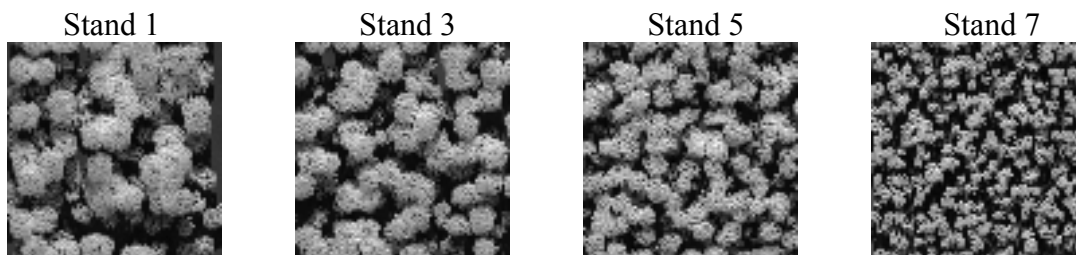


Figure 4. Examples of DART scenes

Lets finally note that among the entire set of modeled scenes provided by Barbier *et al.* (2009), we only used the subset whose acquisition parameters were roughly matching the ones of the real satellite images used in this study (i.e. satellite azimuth angle =  $12^\circ$ , sun elevation angle =  $45^\circ$  and relative sun-sensor angle =  $-180^\circ$ ).

### 2.1.5. Ground control data

#### Plot choice and field data

Forest areas with a homogeneous FOTO-derived texture were identified on a map and plots were positioned with the aim of covering the whole textural gradient. The exact plot positioning within each pre-defined area was left to visual interpretation, once in the field, in order to avoid potential artefacts of the method and to consider the accessibility of each site. Plots geoposition was recorded using a Trimble Juno SB GPS device to locate the plot in the satellite images (see Appendix 2). Each plot was a 100 x 100 m square corrected for topography variations with a Vertex Laser instrument (VL400) and sampled for tree density, diameter at breast height (dbh) or above the buttress for all trees greater than 10 cm dbh and crown position in the canopy (i.e. “emergent”, “high canopy”, “low canopy” or “understory”).

Because the largest trees are more likely to be visible in canopy images, stand structural characteristics were computed from field data each time considering (1) all the trees, (2) only trees greater than 30 cm dbh and (3) only trees greater than 40 cm dbh : density (D), mean tree diameter (Dg or tree of mean basal area), basal area (G). Tree density was also computed from the perspective of trees crown position, considering (1) tree crowns in the higher strata of the canopy (i.e. high canopy + emergent) and (2) tree crowns higher than the understory (i.e. low canopy + high canopy + emergent). Dbh data were also classified into 6 equal-counts bins and the table crossing plots with dbh bins was submitted to a correspondence analysis (CA). The first CA axis (91.64 % of table variance) ranked dbh bins in their natural order from the smallest on its positive side (< 11.5 cm) to the largest on the opposite one (> 32.5 cm). Plots coordinates along this axis were used to summarize dbh distribution. Finally, AGB estimates per plot were computed from dbh data as follow:

$$\text{Ln (AGB)} = a \cdot \text{Ln}(\text{dbh}) \text{ with } a = 1.988422$$

This model choice as well as the “a” parameter value were selected from a previous study of AGB estimation over the study area (Flavenot, 2009). This model proved to yield more accurate AGB estimates when derived from dbh data only.

#### Plot satellite image

In order to integrate ground-data, plots had to be delineated in the satellite images to derive their specific r-spectrum (see 2.2.1 FOTO Overview). This procedure takes into account two main issues: plot aspect (deviation from the N-S axe) and positional error (mainly GPS-induced). In order to cope with these potential biases in the spectral characterizations of plots, instead of extracting a single 125x125m square window per plot (see 2.2.1 FOTO Overview), 4 overlapping windows are extracted to create a half-window size margin error (i.e. 62.5 m) on both North-South and East-West axes (see Fig. 5).

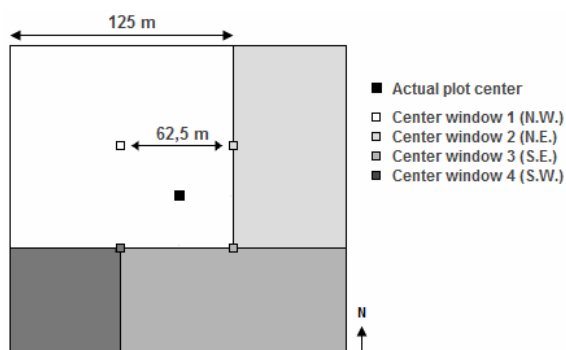


Figure 5. Plot delineation strategy

noticed in the field. This inspection backs up the choice to keep or leave apart a given window from the plot characterization. For example, we see a river path on 3 out of 4 windows extracted over the “F” plot (Fig. 6). This river pattern results in important changes on the spectral characterization of each window, therefore inducing a bias in our plot characterization. Knowing that the plot was not crossed by the river and being able to roughly locate it from the river pattern, we decided to retain only the North-West window for this plot. When no clear feature can be identified, such as on the plot “G” windows (Fig. 6), the spectral characterization is averaged over all 4 windows.

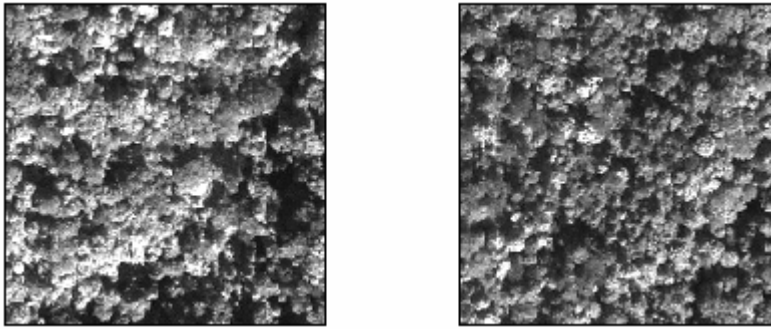


Figure 6. IKONOS images of plot F (left) and G (right). Each image is composed of 4 overlapping 125 x 125 m windows as described in Fig. 5.

By doing so, two plots (F, K) were characterized by the first window only and one plot (I) by the first two.

## 2.2. FOTO method

### 2.2.1. Overview

The method will be partly implemented thanks to the free package “Texturemod” which gathers several Matlab® scripts<sup>2</sup>.

A given run of the method is illustrated hereafter (see Fig. 7). Delineation of non-forest area has to be performed beforehand. The first step is the “windowing” of the images; a grid with window size possibly varying from 19 to 200 pixels is applied to each image. Radial spectra (see 2.2.2) are computed at this scale (i.e. per window) and the radial spectra variation between windows is analyzed with a standardized Principal Component Analysis (PCA). Window scores against the first (e.g. Coueron et al., 2005) up to the three first PCA axes (e.g. Proisy et al., 2007) are then used as textural indices to produce texture maps, which can be correlated with ground measurements. All analyses on windows r-spectra were performed with the R statistical freeware (R Development Core Team, 2008).

### 2.2.2. 2D Fourier Transform and r-spectra

Detailed presentation of 2D Fourier Transform and its application to digital images are available in the literature (Renshaw and Ford, 1984; Mugllestone and Renshaw, 1998), only the main features are developed hereafter.

A digital image is defined as an  $m$  by  $n$  array, say  $\{M_{x,y}\}$  with  $(x=1,\dots,m; y=1,\dots,n)$ , whose cells contain grey scale values in the range of 0 - 255 and express the panchromatic radiance of each pixel in the *spatial* domain. When applying the Fourier transform, we transpose this spectral radiance into the *frequency* domain as a function  $F(p,q)$ , with  $p$  and  $q$  the spatial frequencies (or wavenumbers) traveling in the  $XY$  directions. Fourier coefficients are computed on mean-corrected observations (i.e.  $M'_{xy} = M_{xy} - \bar{M}$ ) as proposed by Mugllestone and Renshaw (1998):

$$a_{pq} = (mn)^{-1} \sum_{x=1}^m \sum_{y=1}^n M'_{xy} \cos[2\pi(px/m + qy/n)]$$

$$b_{pq} = (mn)^{-1} \sum_{x=1}^m \sum_{y=1}^n M'_{xy} \sin[2\pi(px/m + qy/n)]$$

The next step is the computation of the Fourier periodogram as follows:  $I_{pq} = mn(a_{pq}^2 + b_{pq}^2)$ . The value  $I_{pq}/mn$  represents the portion of mean-corrected data variance accounted for by a cosine wave of spatial frequency  $(p,q)$  (Mugllestone and Renshaw, 1998). This periodogram contains information about both scales and directions of the patterns and can be equivalently expressed in polar form, which allows the separation of

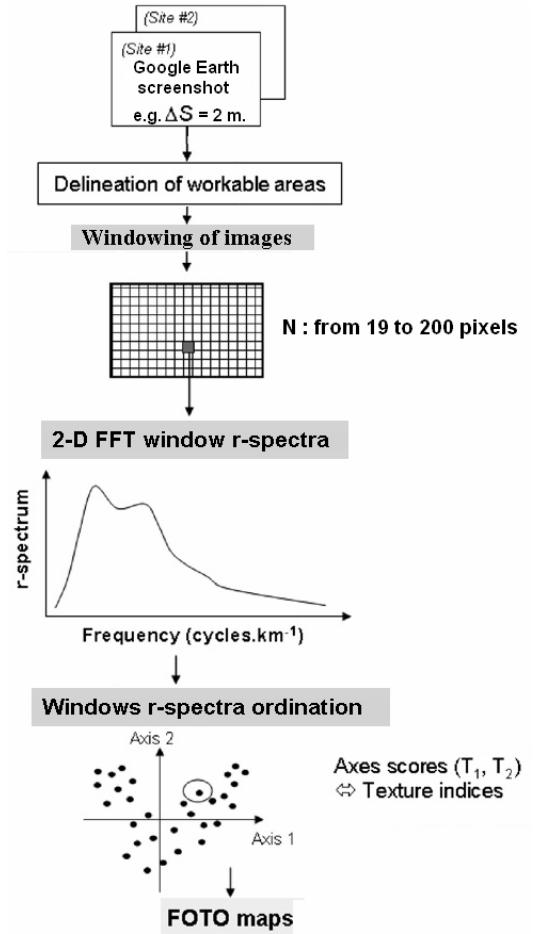


Figure 7. General overview of the FOTO method (from Proisy et al., 2007)

<sup>2</sup> details of Texturemod G.U.I. on <http://amapmed.free.fr/FOTO/>

these two components (r- and o-spectrum).  $I_{r\theta}$  refers to a waveform of spatial frequency  $r = \sqrt{p^2 + q^2}$  and direction  $\theta = \tan^{-1}(p/q)$ . The wavenumber  $r$  is defined as the number of times a pattern repeats itself within the image in direction  $\theta$ . Within the FOTO framework, we only consider the r-spectrum, which is computed by averaging  $I_{r\theta}$  values over all  $\theta$  directions and yield an azimuthally cumulated “radial” spectrum, denoted  $I_r$ . By the way,  $I_r$  values distribution is also suitable for statistical tests. In the absence of spatial structure,  $2I_{r\theta}/\sigma^2 \sim X_2^2$  (with  $\sigma^2$  the image variance; Mugglestone and Renshaw, 1998) and therefore a bin containing  $\theta$   $I_r$  values has its sum distributed as  $X_2^2$  (expected value of  $2\theta$ ).

The radial spectrum is convenient to summarize coarseness-related image textural properties by looking at the way the image variance is decomposed by the successive spatial frequencies (Couteron *et al.* 2002, Couteron *et al.* 2006). Figure 8 (right) shows that an image with a coarse texture will yield a radial spectrum skewed toward small wavenumbers (i.e. large patterns). In this case, the radial spectra display a spike at the 5<sup>th</sup> wavenumber which corresponds to the horizontal periodic pattern (vertical bands) while the high value attached to the 1<sup>st</sup> wavenumber correspond to the vertical linear trend. It is also an interesting feature of the r-spectra that catches image macro-heterogeneity in the first wavenumbers, allowing filtering it. Images with finer texture will yield more balanced spectra and an image with pixel values randomly allocated will yield a spectrum virtually flat (Fig. 8, left).

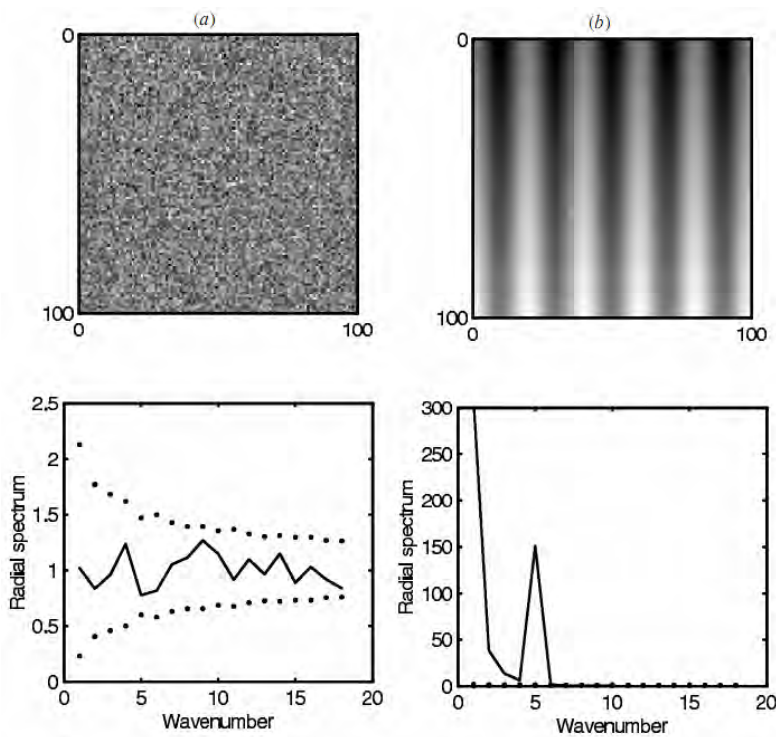


Figure 8. Examples of r-spectra for two images (100x100 pixels): (a) absence of spatial structure, pixel values generated with a Gaussian white noise (WN) with  $\mu=10\sigma$ . (b) Presence of spatial structure generated by the superimposition of a cosine wave (vertical bands) of amplitude  $\beta$ , a linear trend of amplitude  $\beta$  and a WN ( $\sigma=0.1 \beta$ ). The full line represents the r-spectra while the dot line stands for the 5% bilateral confidence interval around 1 (expected value in the absence of spatial structure) (from Couteron *et al.*, 2002).

### 2.2.3. Textural ordination based on r-spectra

The output of the Fourier Transform by Texturemod on one or several images is a single table gathering the  $I_r$  values for all windows (in lines) and per spatial frequencies (in columns, Tab. 4).

Table 4. Output of 2D-FT on a one or several satellite images: PCA data table.

	wavenumber 1	wavenumber 2	wavenumber 3	...	wavenumber n
window 1	$I_{1.1}$	$I_{2.1}$	...		
window 2	$I_{1.2}$	...			
window 3	...				
...					
window m					

Each table line represents the r-spectrum of the given window and displays the grey-scale level variance ( $I_r$ , table cell values) accounted for by increasing spatial frequencies (or wavenumber  $r$ ) from the Nyquist to the lowest resolvable one, in columns. Column-wise standardization is performed and the table is submitted to a standardized Principal Component Analysis, where windows are considered as observations that are characterized by the way their grayscale variance is broken down by the successive spatial frequencies, seen as quantitative variables. The PCA is carried out using the R FactoMiner package (Husson et al., 2009).

Window ordination along these axes composes a gradient that allows us to differentiate windows with respect to their length scale (spatial frequency) distribution and dominance. In other words, canopy scenes are sorted as a function of the presence and dominance of one or more modal spatial frequencies, which can be interpreted as apparent crown sizes (Barbier et al., 2009).

### 2.2.4. Windows r-spectra characterization

Two statistics are used to characterize and compare windows r-spectra. We saw that in the absence of spatial patterning (i.e. random allocation of pixel values), windows yield a virtually flat r-spectrum of known statistical distribution. Since most Earth surface images yield spectra above the confidence envelop, testing against complete randomness (uniform distribution) is of limited interest (Couteron, 2006).

Therefore, to characterize a single (or averaged) r-spectrum, we used the  $D_{\max}$  statistic as proposed by Olier et al. (2005):

$$D_{\max}(x) = \max_{1 \leq i \leq n-1} (\sum_1^i r_i^2 - i/n - 1) \quad \text{with } i \text{ a given spatial frequency and } n \text{ the total}$$

number of spatial frequencies.  $D_{\max}$  measures the position of the maximum deviation between the cumulated r-spectra variance and the null hypothesis of uniform distribution, in a very similar way as Kolmogorov-Smirnov statistics.

In complement to window r-spectrum characterization, we carry out comparisons between windows with the simple log ratio technique. Let  $I_{1(r)}$  and  $I_{2(r)}$  be the r-spectra of two

windows. Under the null hypothesis of identity, the ratio  $R_{(r)} = I_{1(r)} / I_{2(r)}$  is expected to be 1. Deviation from the null hypothesis can be characterized with a confidence envelop built from a Fisher-Snedecor distribution:  $F_{2k,2k}$  with  $k$  the number of periodogram values per spectrum (Diggle, 1990; Couteron *et al.*, 2006).

### ***2.2.5. Image texture – forest structure relationships and mapping***

We relate forest structure parameters to the FOTO textural index (i.e. windows ordination scores along PCA axes) with additive linear models:

$X = a_0 + \sum_{i=1}^j a_i \cdot PCA_i$  with  $X$ : structural parameter,  $a_0$ : intercept,  $a_i$ : regression coefficients of the  $i$  PCA axis and  $j$ : number of PCA axes retained.

The set of modeled canopy scenes (i.e. DART scenes) is used as a cheap and more theoretical data source to assess the quality of the textural index; regression models quality is characterized with adjusted  $R^2$  and AIC criterion (see Appendix 3 for details). The quality of the regression models based on ground truth plots is complemented with relative error (s) and root mean square error (rmse) (Appendix 3).

For analysis and mapping convenience, we perform a K-means clustering (Euclidian distances) on windows coordinates.

## ***2.3. Google Earth vs IKONOS images***

In order to compare outputs from IKONOS and GE, the same window size (in meter) and resulting number of spatial frequencies was used in both cases. The largest class of crown diameter is expected to be about 25 meters in our study area. IKONOS window size was therefore set to 125 1-m pixels (i.e. five repetitions of the largest pattern; Barbier *et al.*, 2009) and GE windows size to 63 2-m pixels. Only the 31 first spatial frequencies were conserved in the IKONOS-derived r-spectra table, corresponding to the spatial frequencies resolvable with GE spatial resolution.

IKONOS images being of higher quality than GE ones (spectral and spatial resolutions), results derived from the commercial image were therefore considered as a reference. The comparison between results derived from the two image types was carried out at the different steps of the analysis with simple linear regressions and scatter plots:

- Textural gradient computation: although direct comparison of unit-window ordination on GE and IKONOS-derived factorial plans may be hampered by differences in total image variances ( $GE \neq IKONOS$ ) or small variations in variables position within each plan, it allows identifying rough trends in windows displacement along the textural gradient.
- Textural gradient sensitivity to topographical variations
- Textural gradient predictive power regarding stand structural parameters

## 2.4. Investigation of topography effect

In a first exploratory step, we carried out linear regressions between window coordinates along the two firsts PCA axes and several environmental variables derived from the DEM in order to identify potential influences. Two types of variables were retained for this report.

Firstly, the mean elevation was used as a basic measurement to check whether elevation itself would influence window ordination. Elevation standard deviation was also used as a proxy for surface heterogeneity.

Secondly, we attempted to build spatial variables that would model the effect of topography variations on canopy texture and therefore allow gathering unit-windows undergoing similar effect. For that purpose, two approaches were adopted:

- (1) A set of variables computed to describe windows exposition to the sun position was used to identify trends.
- (2) An index characterizing the local illumination with respect to the surface and surrounding geomorphology and to the sun position (hillshade model) was created. High hillshade values were found on slopes facing the sun (i.e. illuminated) while slopes facing away from the sun were attributed a low value (i.e. shaded). This illumination index, built upon both elevation data and the sun position, is assumed to be a good modeler of canopy illumination conditions by correlating with changes in the canopy brightness and therefore, at finer scale, in the proportion of tree crown illuminated. Visually, hillshade variations were indeed found to closely match canopy brightness variations (see Fig. 9, full map as Appendix 4).

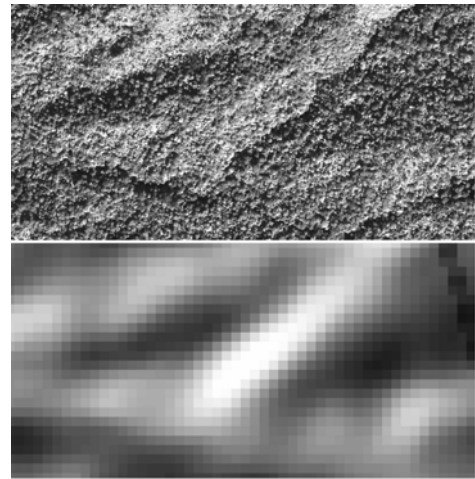


Figure 9. IKONOS (top) and hillshade (bottom) view of a forested scene with marked topography variations.

In a second step, we tried to mitigate the r-spectra variability due to topography variations by performing a so-called partitioned standardization (Barbier *et al.*, 2009). The spatial variable showing the strongest influence over the textural gradient is divided into  $n$  bins (K-means clustering on Euclidian distances) and unit-windows are allocated to their respective bin. Bins are standardized separately and then pooled together to perform the PCA. By doing so, we attempted to normalize windows r-spectra regarding the different canopy illumination conditions resulting from variations in the underlying terrain, and regardless of the canopy grain. It is therefore important that each bin encompasses the whole canopy textural gradient.

The last step consists of assessing the effect of this partition process on the influences of environmental variables on the PCA axes and is carried out with simple linear regressions.

### 3. Results

We first carry out the textural analysis on the reference IKONOS image type (3.1) prior to the comparison of the derived textural gradient to the one from the cheaper GE alternative (3.2). Effects of topography (3.3) as well as FOTO index relationships with stand structural parameters (3.4) are later on presented for both image types with an emphasis on IKONOS-derived results.

#### 3.1. Textural analysis

The PCA run over the r-spectra table yielded a prominent first axis explaining more than 40% of the variation between windows, while the second and third axes only explained 6.6% and 3.7%, respectively (Fig.10. up-left). We therefore retained the first plan formed by axes 1 and 2 which positioned windows in a slight “horseshoe” shaped cloud similarly to previous FOTO applications (e.g. Proisy, 2007). The circle of correlation between variables (spatial frequencies) and the two first axes (Fig.10.up-right) also displayed an expected pattern with the lowest spatial frequencies ( $f < 30 \text{ cycles.km}^{-1}$  or  $\lambda > 30\text{m}$ ) on the negative side of the first axis and the highest ( $f > 100 \text{ cycle.km}^{-1}$  or  $\lambda < 10\text{m}$ ) on the opposite one. Intermediate spatial frequencies were correlating with the positive side of the second axis.

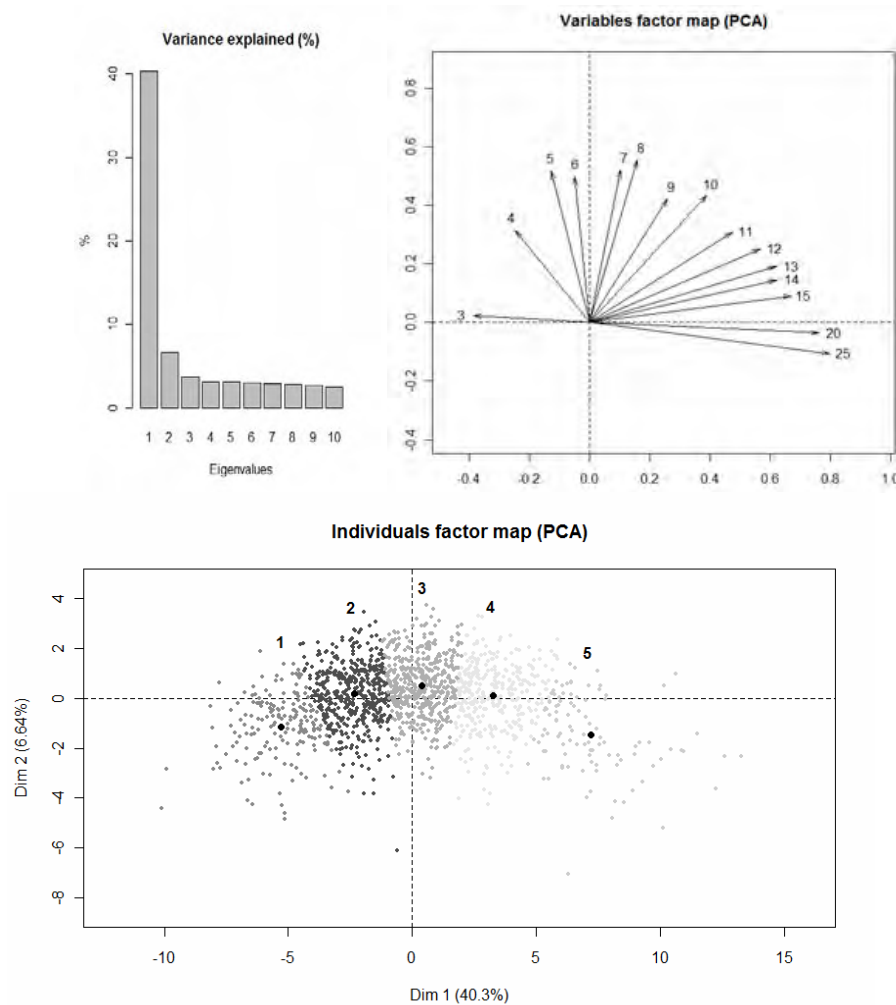


Figure 10. Main PCA results: (up-left) Eigenvalues histogram expressed in percentage of variance explained, only the 10 first values are plotted; (up-right) correlation circle of spatial frequencies with PCA axes, selective spatial frequencies above the 15<sup>th</sup> wavenumbers for visibility; (bottom) first factorial plan with 5 clusters, solid black circles illustrate clusters barycenter.

A K-means clustering was performed on window coordinates and the resulting clusters were forming a gradient over the first axis, as shown by the position of their barycenters (Fig. 10. bottom). Spectral analyses carried out on the averaged cluster r-spectra underlined the differences of spatial frequencies distribution and dominance that characterize the range of textural patterns found across this gradient.

Figure 11 (top) shows the averaged clusters' r-spectra and is computed on standardized data (i.e. for a given spatial frequency, relatively to the whole window-set). It illustrates the successive dominance of clusters among spatial frequencies, with the first cluster scoring relatively higher over low frequencies ( $f < 24 \text{ cycles.km}^{-1}$  or  $\lambda > 41\text{m}$ , texture dominated by large patterns) to the 5<sup>th</sup> over high frequencies ( $f > 65 \text{ cycles.km}^{-1}$  or  $\lambda < 15\text{m}$ , texture dominated by small patterns).

The spatial frequency characterizing the maximum deviation between the cluster averaged r-spectra and a uniform distribution ( $D_{\text{max}}$ , computed on raw r-spectra) were indeed increasing from the 1<sup>st</sup> to the 5<sup>th</sup> cluster with 40, 65, 81, 81 and 105 cycles.km<sup>-1</sup> respectively, which corresponds to pattern sizes of 25, 15.5, 12.5, 12.5 and 9.5m. Although  $D_{\text{max}}$  parameter did not differentiate clusters 3 and 4, the ratio of their r-spectra show significant differences with cluster 4 scoring significantly lower for spatial frequencies below 50 cycles.km<sup>-1</sup> or  $\lambda > 21 \text{ m}$  and higher above 70 cycles.km<sup>-1</sup> or  $\lambda < 14 \text{ m}$  (see Fig. 11, bottom).

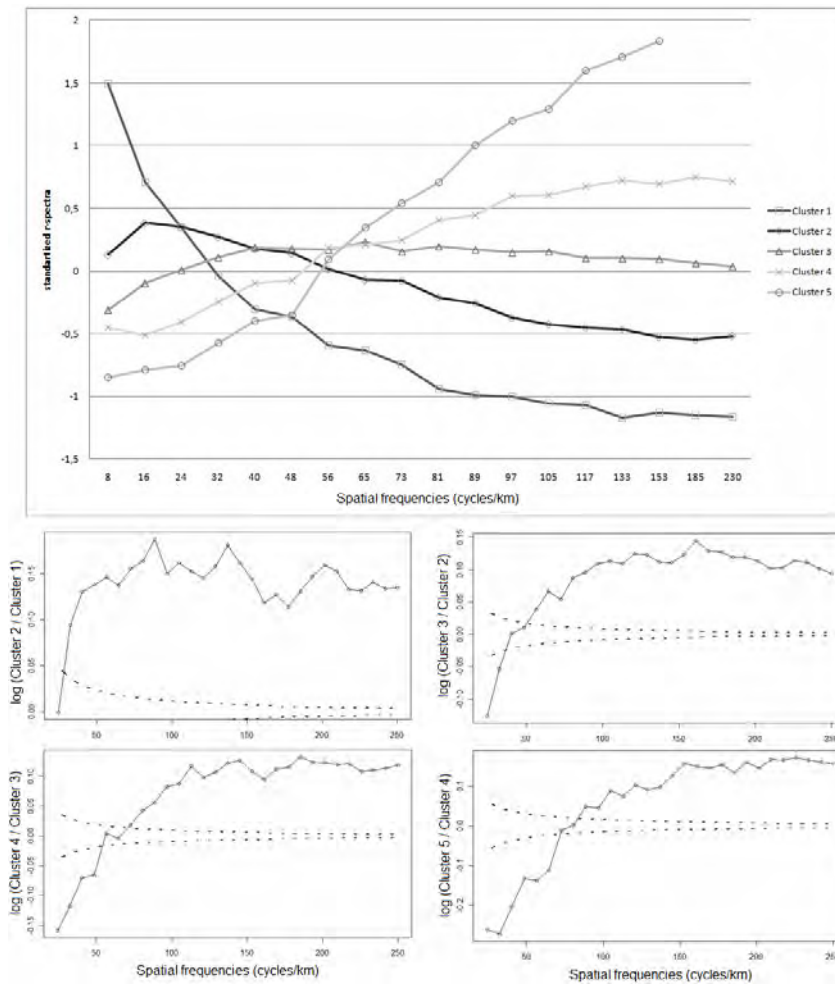


Figure 11. (top) Averaged standardized clusters r-spectra (bottom) Ratio of averaged r-spectra for successive cluster (solid line) and 5% bilateral confidence interval (dot line).

We have shown that our textural ordination is able to discriminate forested scenes (i.e. unit-windows of IKONOS image) according to the dominance of a range of spatial patterns in the image texture. In order to test the relationship between these textural patterns and forest structural parameters of interest such as stand average crown size, we used DART scenes as supplementary individuals in our factorial plan (Fig. 12).

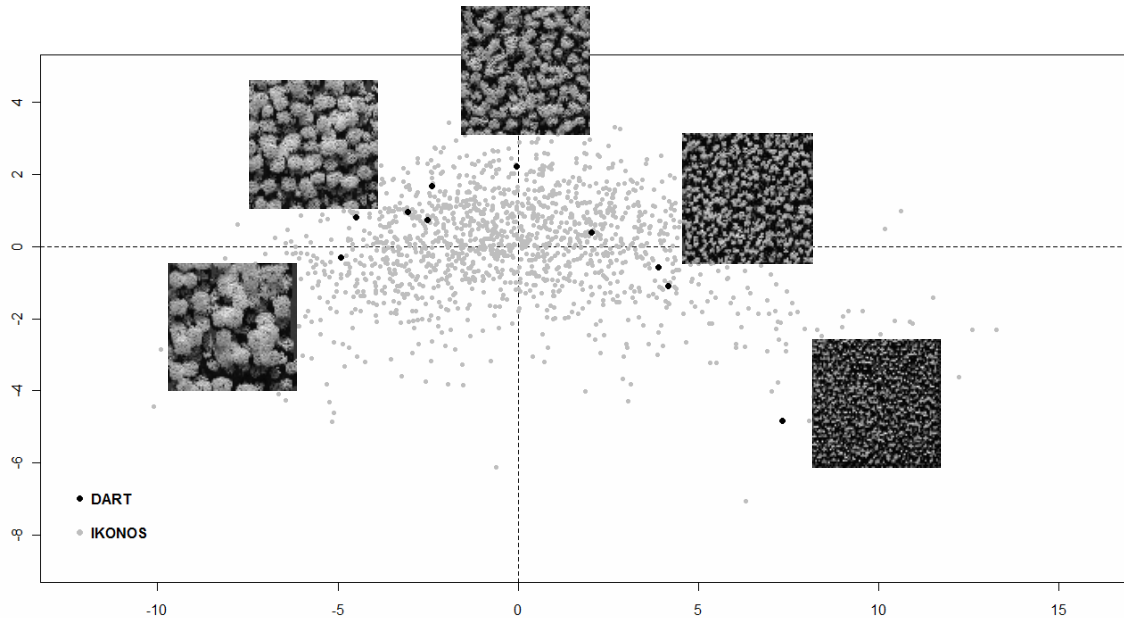


Figure 12. DART scenes as supplementary individuals in the IKONOS-derived factorial plan.

Once plotted on the first factorial plan, the modeled scenes were distributed over the large majority of the first axis gradient, providing us with insights on the structural range this axis is theoretically able to discriminate. Indeed, for e.g. crown diameters, windows ordinated below -4.5 on this axis may be dominated by trees with crown diameters  $> 20$  m while windows placed above the 7.5 ordinate might be dominated by trees with crown diameters  $< 7.5$  m.

We used the scene coordinates along the axes as textural indices to test the quality of the ordination for forest structure prediction (see Fig. 13).

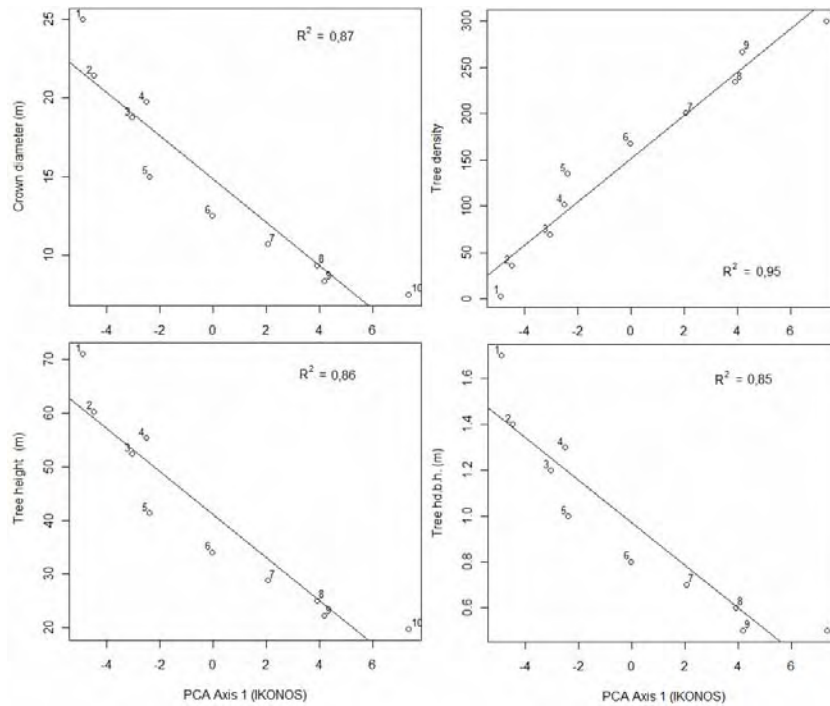


Figure 13. DART modeled structural parameters as a function of DART scenes' coordinate along the first PCA axis used as a textural index. Stand numbers label the observations (see Table X). All adjusted  $R^2$  values are significant ( $p$ -value  $< 0.001$ ).

When considered separately, the first axis was a good predictor of all structural parameters with all adjusted  $R^2$  values above 85% while the second axis did not significantly explain structural variance among windows. Indeed, window ordination along the second axis is not as clear as in the case of the first axis. Barbier *et al.* (2009) considered that the second axis provides us with information on the homogeneity of the structure within the window (i.e. the higher the distance to the origin is, the more homogeneous is the window structure). The relationship between forest structure (response variable) and structure homogeneity, and all the more with the second axis alone (used as predictor variable) is poor and logically lead to un-significant regression results. However, the second axis did improve structure predictions when used in combination with the first axis yielding all adjusted  $R^2$  up to 97% and lower AIC criterion values than with only A1 (see. Tab. 5).

Table 5. Linear regressions between scene structure parameters and IKONOS-derived textural indices (model 1: first PCA axis used as predictive variable; model 2: 2 first PCA axes used as predictive variables)

	model 1 (~ A1)		model 2 (~ A1 + A2)	
	adj. $R^2$	AIC	adj. $R^2$	AIC
Crown diameter	0,87	17,68	0,97	3,62
Tree density	0,95	64,49	0,97	58,46
Tree height	0,86	39,49	0,97	25,30
Tree d.b.h.	0,85	-34,54	0,97	-48,92

### 3.2. Google Earth-derived textural gradient

The first principal component of the PCA based on Google Earth-derived windows r-spectra explained a similar percentage of variance (40.1%) as in the cases of r-spectra derived from the IKONOS commercial image, while the second axis was slightly heavier (10.1% ; see. Fig. 14).

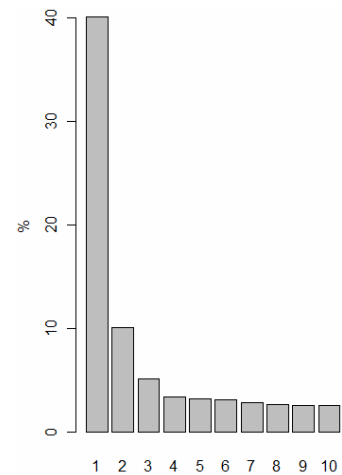


Figure 14. Eigenvalues histogram (expressed in % of variance)

In terms of window ordination, Figure 15 shows that in the case of the first axes, GE-based windows ordinates are reasonable predictors of IKONOS-based ones with an adjusted  $R^2$  of nearly 50% ( $p$ -value < 0.001,  $rmse=2.5$ ), no apparent systematic bias and a similar range of error all along the axis. There are however major differences

of windows ordination along the second GE-based and IKONOS-based axes with an adjusted  $R^2$  below 5% ( $p$ -value < 0.001,  $rmse=1.7$ ) and a high variance around the regression trend (Fig. 15, right). This linear trend also greatly differs from a  $x=y$  line (i.e. ideal match between GE and IKONOS-derived window ordination) and the regression line on smoothed data is virtually plane below the -2 ordinate on GE axis. Such differences may indicate that even though GE-based 2<sup>nd</sup> PCA axis explains more r-spectra variation among windows, it may not carry the same information as the IKONOS-based 2<sup>nd</sup> axis or contains irrelevant information in terms of canopy texture (noise).

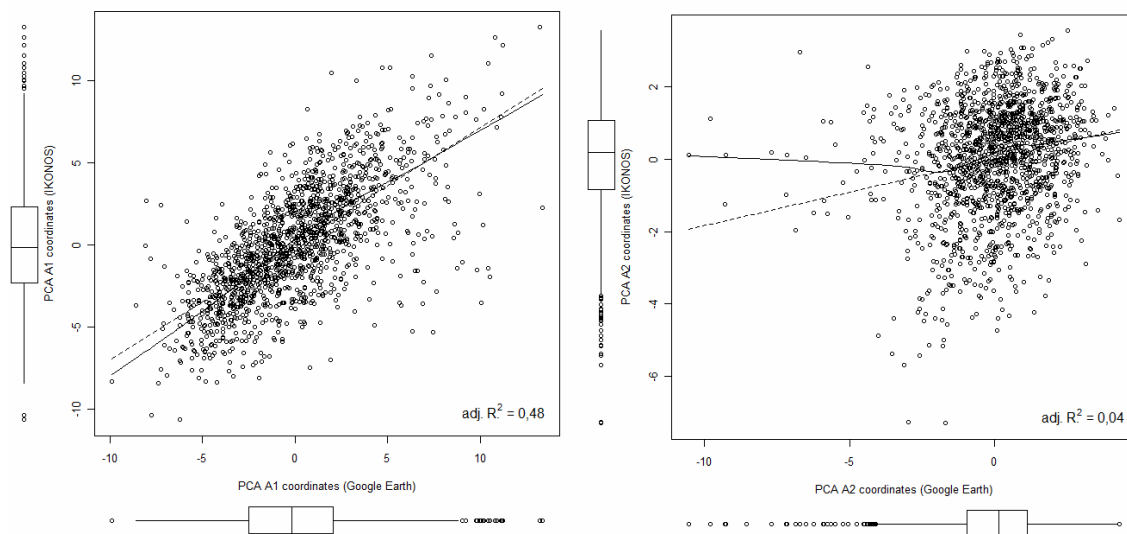


Figure 15. IKONOS-based windows ordinates as a function of GE-based ones (dotted line: regression line, full line: non-parametric regression on smooth data (locally-weighted polynomial regression))

We detailed the IKONOS – GE comparison by looking at the trends of windows displacement on the PCA axes from GE to IKONOS factorial plans (Fig. 16). On A1, about 34% of the windows are displaced by less than 1 unit, 6% by more than 5 units and the overall median is about 2 units. The large majority of the windows were ordinated between -5 and 5 and a slight trend appear with windows positively ordinated on this axis range (close to 5) being displaced toward a more negative ordination on IKONOS (i.e. “GE > IKONOS”) and the other way around in the negative side of the range (i.e. “IKONOS > GE”). This very same

trend is increased for windows ordinated at the edges of the axis (i.e. above 5 or below -5) with displacements up to 13 units.

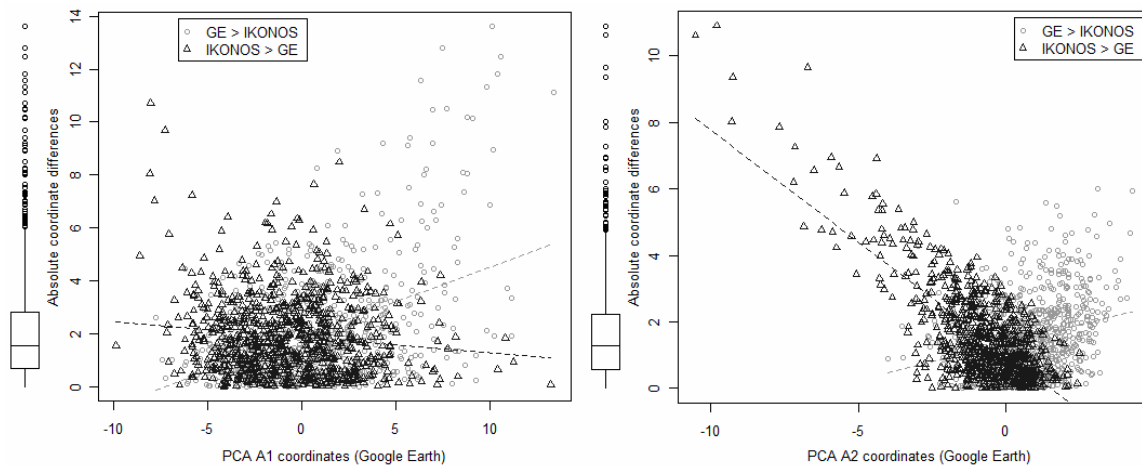


Figure 16. Difference trends between GE and IKONOS-based ordinations (dotted line: linear regression line)

Examples of windows concerned by such important displacement from one factorial plan to the other are plotted in the figure below and the visual inspection of their canopy grains confirms the higher quality of the textural gradient derived from IKONOS.

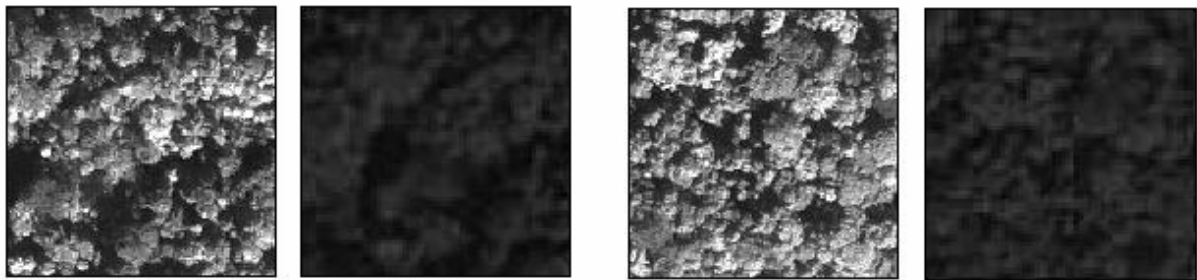


Figure 17. IKONOS and GE view of windows undergoing an important displacement from the GE to the IKONOS-derived PCA first axis: (left) window ordinated as a very coarse grain on GE (PCA1=-8) and as an intermediate grain on IKONOS (PCA1=0); (right) window ordinated as a very fine grain on GE (PCA1=13) and as an intermediate grain on IKONOS (PCA1=2).

The canopy grain of the left window is slightly coarser than the right one, although its more complex structure (tree height heterogeneity) creates larger shades and makes the distinction of large tree crowns easier. The fine scale illumination variations that allow the recognition of crowns or branches limits in dense/homogeneous window parts disappear with the lost of spatial details from IKONOS to GE, while the visual importance of moderate to large shade remains.

Windows displacement on the 2<sup>nd</sup> axes of the PCA display the same trends as in the case of the first axes although it is visually more pronounced (Fig. 16 - right). On this axis, 41% of the windows are displaced by less than 1 unit and about 2% by more than 5 units. Displacement on this axis is however quantitatively more important than on the first axis given its smaller range.

Alongside the differences of windows ordination between the two image types, it is noteworthy underlining the limited spectral range of GE images. Indeed, even though both image types are displayed in 0-255 grayscales, averaging GE RGB true color bands result in actual input data range tremendously smaller than the IKONOS input range (Fig. 18).

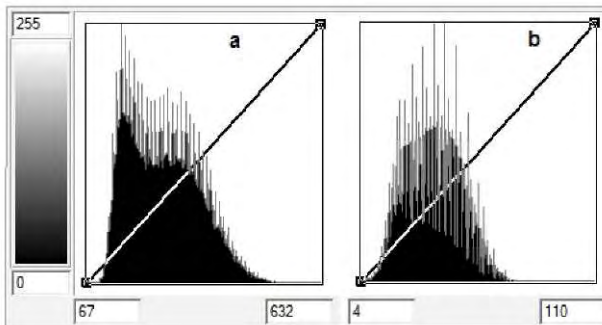


Figure 18. Transform histogram of (a) IKONOS and (b) GE pixel values over the top part of the study area. The X axis displays the actual input data values.

Finally, DART scenes were also used to study the quality of the GE-derived textural indices. The virtual scenes were ordinated at very similar positions on the first G.E. and IKONOS axes and differed in their ordination on the 2<sup>nd</sup> axes. Therefore, we obtain the very same regression scores between the textural indices based on the first axis only and structural parameters as we obtained with the IKONOS image. Regressions based on the model including the second axis also lead to a slightly better fit of the models to observed data and lower AIC criterion values (see Tab. 6). We can however expect a decrease of the second axis explanatory power with a larger model calibration sample size, due to the apparent noise it seems to contain.

Table 6. Linear regressions between scene structure parameters and GE-derived textural indices (model 1: first PCA axis used as predictive variable; model 2: 2 firsts PCA axes used as predictive variables)

	model 1 (~ A1)		model 2 (~ A1 + A2)	
	adj. R <sup>2</sup>	AIC	adj. R <sup>2</sup>	AIC
Crown diameter	0,87	17,52	0,93	12,69
Tree density	0,95	64,20	0,96	63,45
Tree height	0,87	39,33	0,92	34,52
Tree d.b.h.	0,85	-34,68	0,92	-39,96

### 3.3. Effect of topography

#### 3.3.1. Local effect

Detailed investigations of windows ordination along the PCA axes with regards to their specific canopy grain allowed us to identify a first bias introduced at the window level (local effect). Indeed, abrupt topographic variations may lead in some cases to sudden changes in canopy texture as observed by the sensor. Figure 19 (left) illustrate one of those varying cases, with a slope going steeply down from South-Est to North-West and abruptly raising up in the same direction. The sun azimuth position ( $148^\circ$ ), roughly in line with the slope aspect, maximizes the difference in canopy texture observable on each hill. Windows that happened to encompass two different types of texture (Fig. 19, right) seemed to be inconsistently ordinated along the first PCA axis. In the given example, the window scores -7.6 on the first PCA axis, which correspond to a very coarse canopy grain whereas its grain would be visually characterized as barely intermediate.

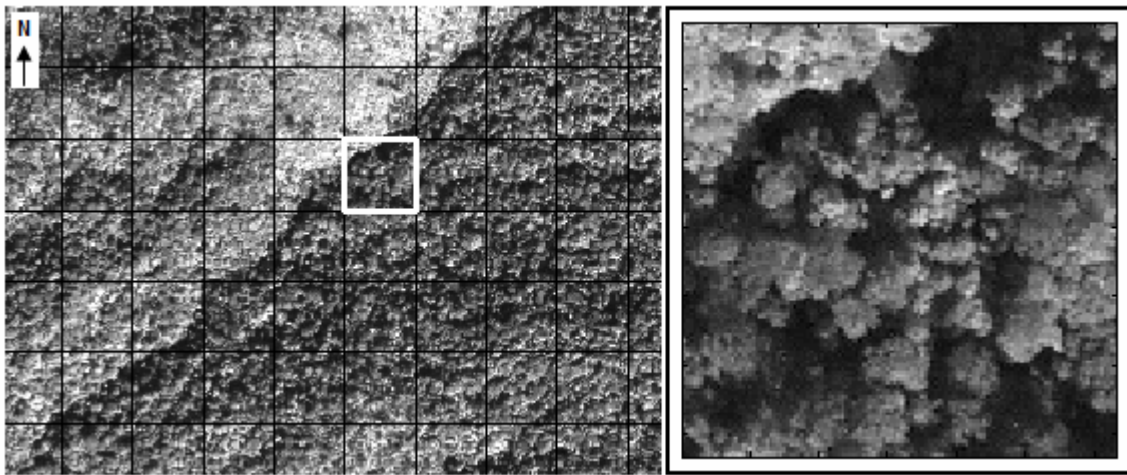


Figure 19. Influence of abrupt slope changes on window texture. (left) Area displaying two steep slopes of opposite aspects and (right) example of window encompassing textural types.

Windows located on such textural change were identified on the satellite image and were roughly found on the same quadrant of the factorial plan (Fig. 20, top-left) regardless of their canopy grain (Fig. 20, bottom).

The mean r-spectra of this window group shows that relatively to the whole window set, their variance is broken down into the two firsts spatial frequencies mainly (Fig. 20, top-right), which could be explained by the high macro-heterogeneity they contain, while higher frequencies that could describe the canopy grain do not explain any image variance. Those windows therefore end-up being ordinated regarding this macro-heterogeneity (i.e. correlate with the first spatial frequencies, negative side of the first PCA axis) rather than their canopy grain.

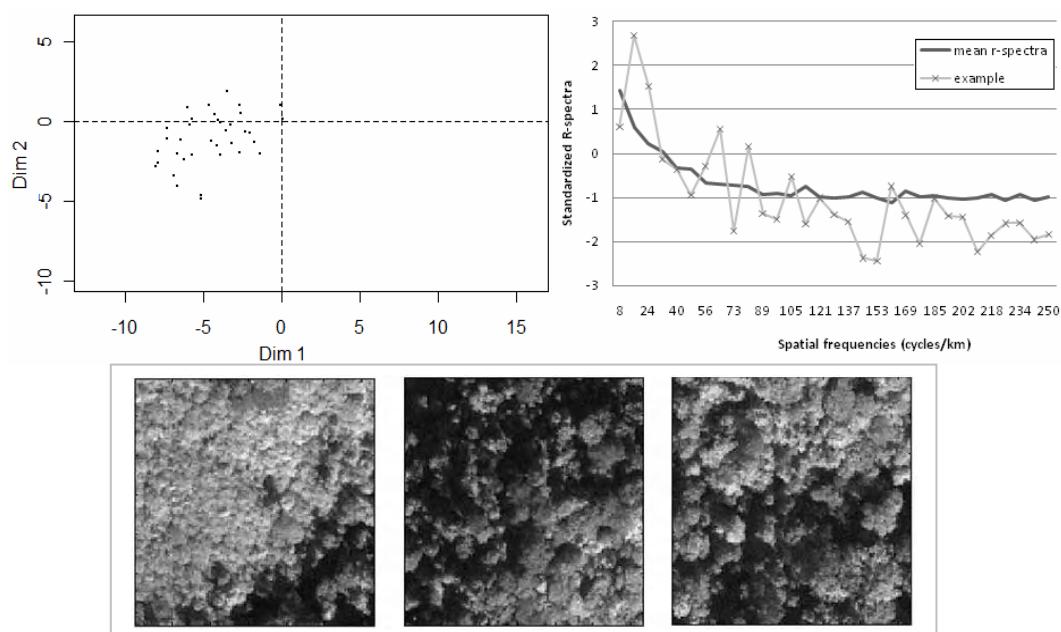


Figure 20. (top-left) Position of windows encompassing two types of canopy texture on the IKONOS-derived first factorial plan, (top-right) standardized R-spectra of this window group (mean) and of window presented in Figure X and (bottom) examples of such windows displaying different canopy grain.

The proportion of such windows depends on the geomorphologic set up of the studied scene and the position of the sun. It has been quantified to less than 3% (n=36) on the northern part of our study area (19 km<sup>2</sup>), which presents however marked topographic variations. Because of its size, this group of windows displaying a particular illumination pattern do not have major influence on PCA axes computation and therefore on our textural gradient. It is noteworthy that the same problematic windows were found on IKONOS and GE images.

### 3.3.2. Global effect

The good regression scores found between the textural gradient and different DART scenes parameters prior to any topographic correction suggest that topography variations do not induce major biases in the computation of this textural gradient. However, we found that the selected environmental variables do influence the PCA axes. The mean elevation as well as its standard deviation were significant predictors of the IKONOS-derived first axis ( $R^2$  adj. of 0.09 and 0.05 respectively) and had no influence over the second one (Tab. 7). Figure 20 (left) shows that windows with high elevation tend to be ordinated negatively on the first axis and the other way around. A similar, though weaker trend was found on GE first axis with  $R^2$  adj. of 0.02 and 0.01 for elevation mean and standard deviation respectively. It was unexpected to find that the later variables also had important influences on GE 2<sup>nd</sup> axis, with  $R^2$  adj. of 0.22 (see Fig. 21 - right) and 0.04, respectively.

Table 7. Influence of elevation mean and SD on window ordination scores (derived from IKONOS and G.E. images).  $R^2$  adj. with significance level (p-value: \*\*\* < 0.1%; \*\* < 1%; . < 10%)

	IKONOS		Google Earth	
	Dim 1	Dim 2	Dim 1	Dim 2
Elevation (mean)	0.092 ***	0.001	0.019 ***	0.217 ***
Elevation (SD)	0.045 ***	0.000	0.009 ***	0.042 ***

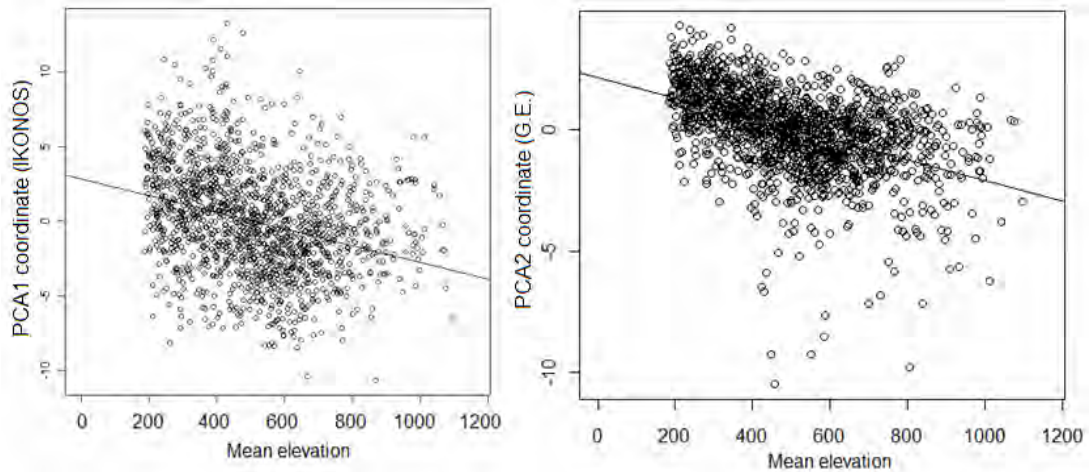


Figure 21. Influence of mean elevation on IKONOS 1<sup>st</sup> axis (left) and GE 2<sup>nd</sup> axis (right)

Spatial variables computed to describe the effect of topography-induced illumination variations on the canopy also correlated with the PCA axes. The set of manually parameterized variables characterizing window dominant facet aspect regarding the sun position (i.e. face, face away, else) coupled or not with slope data displayed the same trends with different levels of significance. The combination of the more “tolerant” aspect variable (i.e. Aspect 3) with slope data lead to the best results (Tab. 8) and show that on GE and IKONOS-derived PCA1, windows facing the sun tend to be ordinated toward the positive side of the axis while windows facing away to the sun toward the negative one (Fig. 22). While GE-derived PCA2 did not seem to be influenced by this set of variables, IKONOS-derived PCA2 displayed the opposite trend than the first axis.

Table 8. Relationships between PCA axes and spatial variables manually computed (Aspect & Combined data). Windows are divided among 3 groups (1: face away to the sun, 2: else, 3: face the sun) and multiple mean comparison tests are carried out (Kruskal & Wallis:  $X^2$  value, Tukey: t-value). Significance levels coded as follow: \*\*\* < 0,1%; \*\* < 1% ; \* < 5% ; . < 10%.

	IKONOS							
	Dim 1				Dim 2			
	Kruskal & Wallis	Tukey post-hoc test			Kruskal & Wallis	Tukey post-hoc test		
	$X^2$	2 - 1	3 - 1	3 - 2	$X^2$	2 - 1	3 - 1	3 - 2
Aspect 1	13.2 **	-1.5	-2.1 .	-2.9 **	51.6 ***	1.5	2.8 *	6.5 ***
Aspect 2	23.6 ***	-1.7	-2.8 *	-4 ***	76 ***	3.2 **	5.1 ***	7.6 ***
Aspect 3	40.3 ***	-2.2 .	-3.9 ***	-5.2 ***	101.2 ***	3.8 ***	6.6 ***	8.7 ***
Combined data	71.7 ***	-2.5 *	-4.7 ***	-7.3 ***	83 ***	3.1 **	5.6 ***	8 ***

	Google Earth							
	Dim 1				Dim 2			
	Kruskal & Wallis	Tukey post-hoc test			Kruskal & Wallis	Tukey post-hoc test		
	$X^2$	2 - 1	3 - 1	3 - 2	$X^2$	2 - 1	3 - 1	3 - 2
Aspect 1	8.8 *	-1.5	-1.8	-1.5	3.8			
Aspect 2	22.7 ***	-2.4 *	-3.1 **	-2.8 *	5.6 .	1.9	1.7	-1
Aspect 3	43.2 ***	-2.4 *	-4 ***	-4.6 ***	2.2			
Combined data	54 ***	-2.5 *	-4.2 ***	-5.3 ***	3.3			

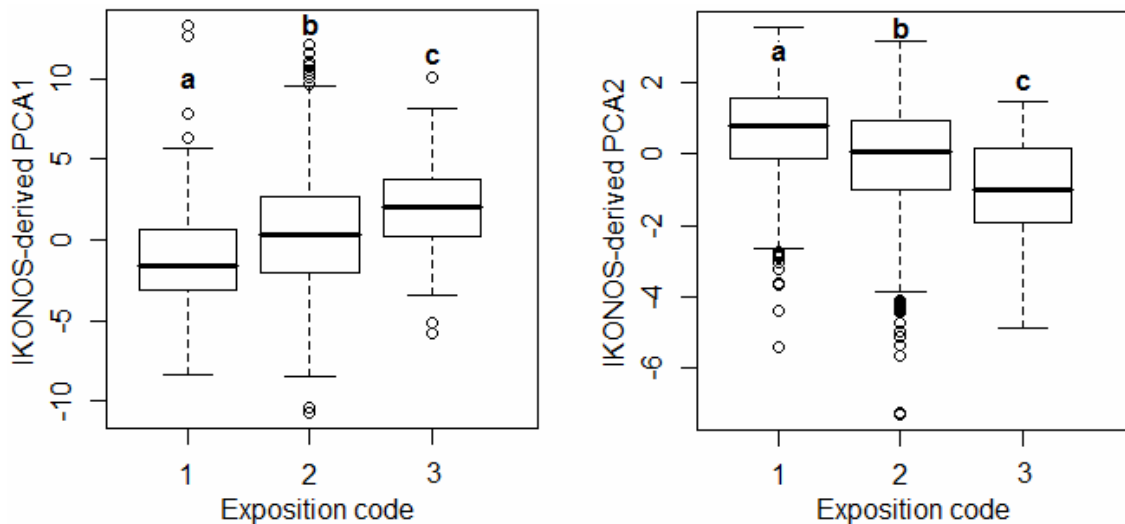


Figure 22. Influence of Combined data on IKONOS-derived PCA1 (left) and PCA2 (right). Exposition codes divide windows among the ones facing the sun (3), facing away (1) and else (2); only the subset of windows characterized by a slope between 20.4° and 60.4° is considered. Letters (a, b, c) correspond to significant results of Tukey post-hoc tests.

The hillshade index consistently described the same trends (Tab. 9, Fig. 23 – top). Windows with high mean hillshade (i.e. illuminated) tend to be ordinated positively on the first axis and the other way around (see Fig. 23). This trend confirm the hypothesis that on the illuminated side of the hill, trees display smaller shades and may be confuse with smaller trees while on the shaded side of the hill, tree shades are larger which induce a confusion with larger trees. The regression line on smoothed data show that this trend is more pronounced on the second half of the hillshade gradient. Indeed, one can imagine that a tree located on a hill facing away to the sun will have a larger shade only if he is directly hit by light rays. Therefore, trees on steeps slopes facing away to the sun may only be illuminated by the diffuse illumination and not display shade at all. The PCA 2<sup>nd</sup> axis displayed the opposite trend with the brightest windows being negatively ordinated, which could indicate a greater textural heterogeneity. GE-derived axes were similarly influenced by hillshade variations, although the relationships are weaker.

Table 9. Influence of mean hillshade on window ordination scores (derived from IKONOS and G.E. images). R<sup>2</sup> adj. with significance level (p-value: \*\*\* < 0.1%).

	IKONOS		Google Earth	
	PCA 1	PCA 2	PCA 1	PCA 2
Hillshade (mean)	0.095 ***	0.068 ***	0.046 ***	0.015 ***

The hillshade gradient was divided into a subjective number of bins (6 bins, K means clustering). The underlying idea was to obtain a reasonable number of bins so that they may encompass the whole canopy textural gradient while displaying at the same time significant differences in term of ordination on the factorial plan. A multiple mean comparison test (Tukey) was used (Fig. 23 – bottom) and the 3 firsts bins were pulled together (Fig. 24, left).

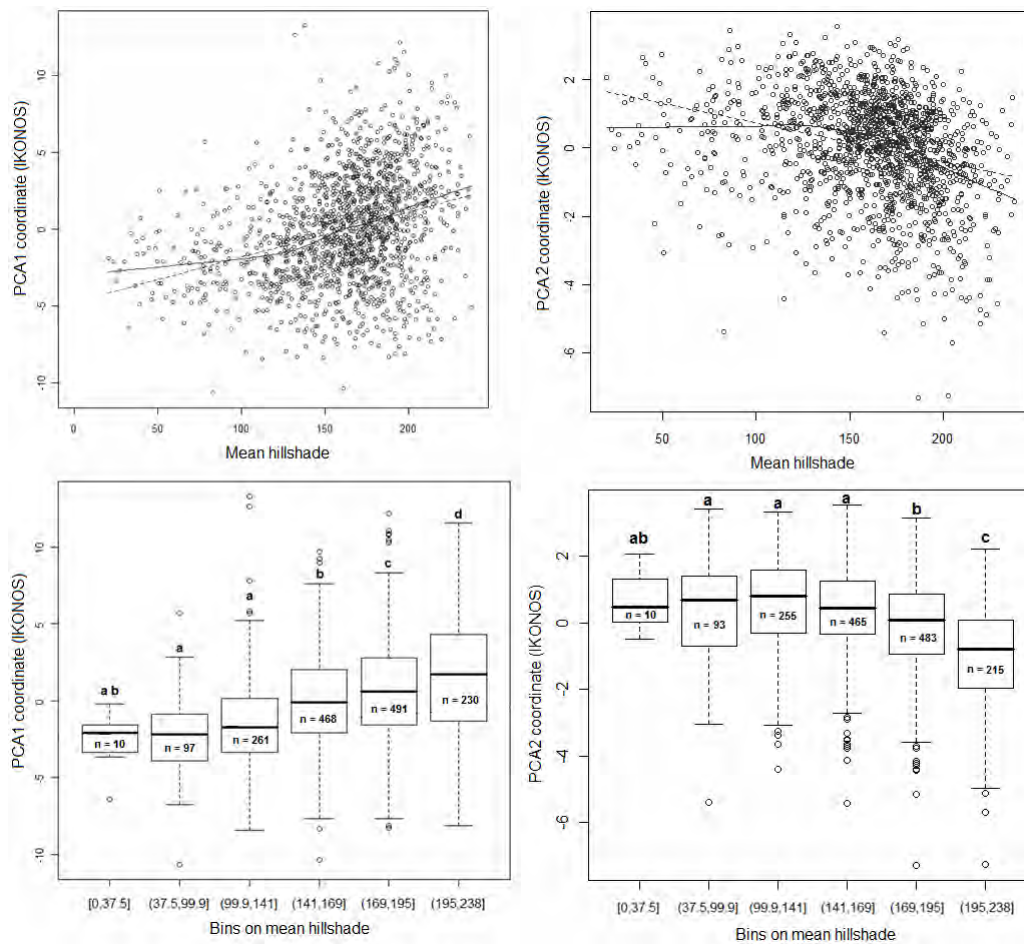


Figure 23. (top) Regressions of mean hillshade on windows coordinate along PCA1 (right) and PCA2 (left); dotted lines: linear regression, full lines: non-parametric regression on smooth data; (bottom) Initial bins on mean hillshade (K mean clustering on Euclidian distance) and Tukey post-hoc test results.

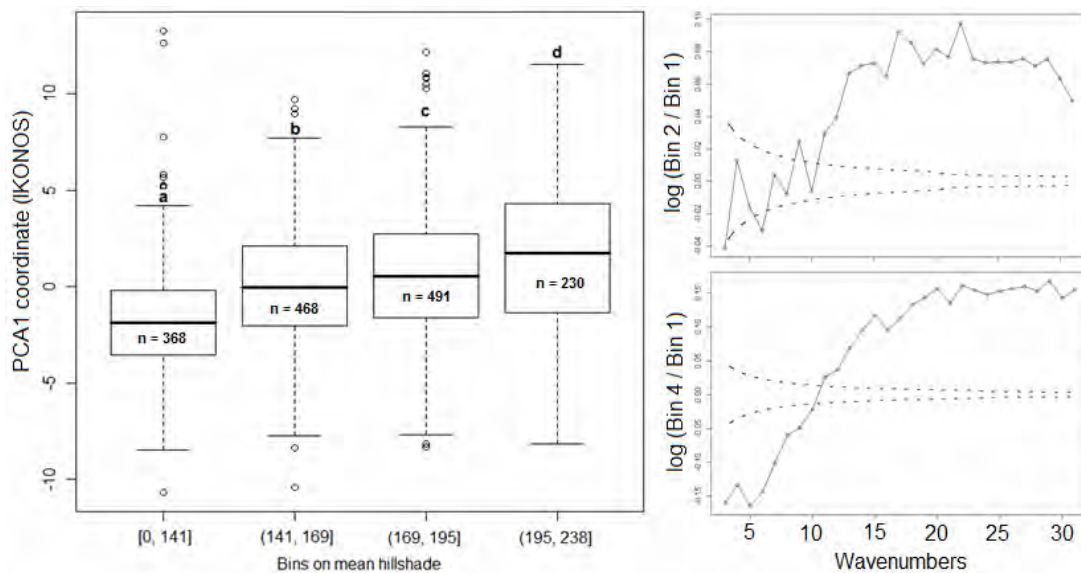


Figure 24. (left) Final bins on mean hillshade and Tukey post-hoc test results; (right) Log ratio technique on the 2 first (top) and 2 extreme (bottom) bins; full lines: log ratio, dotted lines: point-wise confidence interval computed from a F-distribution.

A comparison of the mean bin r-spectra show that when we consider two successive bins (e.g. 1 and 2, Fig. 24, right-top) or windows set, the brightest one have significantly higher scores over high frequencies (starting from 90 cycles.km<sup>-1</sup> or  $\lambda = 11.3$  m) and no significant differences appear over lower frequencies while when the hillshade difference increase between the bins (e.g. 1 and 5, Fig. 24 right-bottom), the brightest one also display significantly lower scores over the low frequencies.

A partitioned standardization was performed and allowed removing the unwanted influences of the hillshade (Fig. 25, left) as well as the Aspect and Combined variables on the textural gradient. The influences of elevation mean (Fig. 25, right) and standard deviation were mitigated but still very significant ( $R^2$  adj. of 0.035\*\*\* and 0.003\*\* respectively). Similar results were observed on the GE-derived textural gradient with the total disappearance of the hillshade influence on both PCA axes, the mitigation of mean elevation ( $R^2$  adj. = 0.003, p-value < 5%) and disappearance of elevation standard deviation influences on the first axis. The two latter variables conserved however important influences on the 2<sup>nd</sup> PCA axis with  $R^2$  adjusted of 0.167 and 0.016 (p-values < 0.1%) for elevation mean and SD respectively.

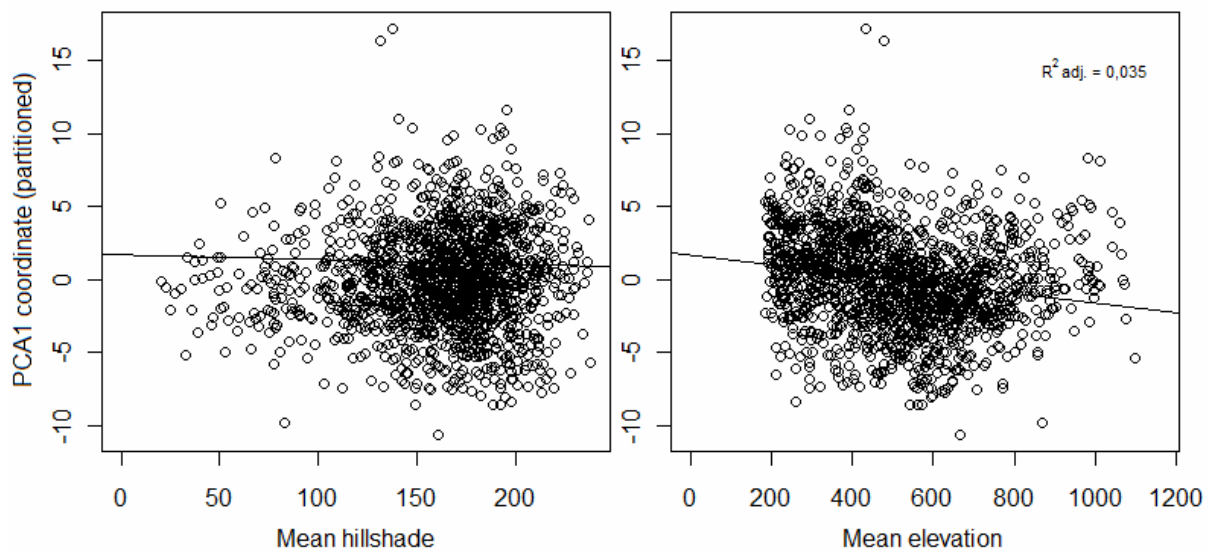


Figure 25. Regression of mean hillshade (left) and mean elevation (right) on window coordinate along PCA1 after partitioned standardization (IKONOS).

We used the PCA results from this partitioned approach later on the analysis.

### 3.4. Predicting stand structure parameters

#### 3.4.1. Plots structure

Plot overview (IKONOS) and location within the study area is presented in Appendix 2.

Plots G, I and P, J, K were sampled in November 2009 and January 2010 respectively. We also extracted structural data along with location coordinates for two more plots in the IFP database: H (2009) and F (2005).

Tables 10 and 11 summarize plots structural parameters as used for the model calibration. Variables considering only trees greater than 30 and 40 cm dbh led to similar results, the latter set of variables is therefore left away for clarity purpose.

Table 10. Stand structure parameters collected for 7 1-ha ground-truth plots (horizontal distance) close to the Uppangala village (Western Ghats, India).

Plots	Density (D, trees.ha <sup>-1</sup> )		Basal area (G, m <sup>2</sup> .ha <sup>-1</sup> )		Mean tree diameter (Dg, cm)	
	> 10 cm dbh	> 30 cm dbh	> 10 cm dbh	> 30 cm dbh	> 10 cm dbh	> 30 cm dbh
K	381	16	10.28	2.47	17.93	44.29
J	517	25	12.84	3.48	18.55	42.08
P	539	178	54.38	44.12	35.16	56.18
I	371	87	21.84	15.45	27.02	47.54
F	577	106	29.57	18.81	25.54	47.53
G	567	143	36.31	25.64	28.97	47.78
H	624	150	50.02	39.46	31.95	57.87

Table 11. AGB estimates and CA1 plot scores (see fig 27, left)

Plots	AGB (t. DM. ha <sup>-1</sup> )	Diametric structure (CA1)
K	126,28	0,42
J	157,80	0,48
P	661,06	-0,40
I	266,60	-0,05
F	361,09	0,01
G	442,97	-0,23
H	608,36	-0,08

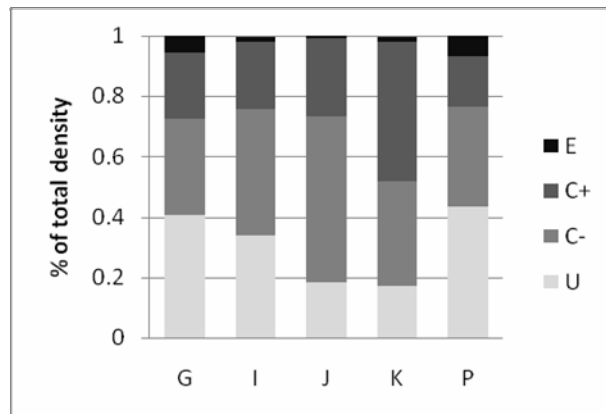


Figure 26 Relative tree density in function of tree crown position (E : emergent, C+ : high canopy, C- : low canopy, U : understorey).

We attempted to cover the canopy textural gradient extremities with plots J and K (very fine canopy grain) and plot P (very coarse canopy grain). This is indeed apparent in Figure 26 (right) with J and K largely dominated by small trees (< 15cm dbh) while P have the more balanced distribution over the dbh bins. The long-known plots H and F were judged as coarse and intermediate (respectively) by experienced IFP staff. We therefore tried to sample a replicate for the coarse grain (G) and a fine grain (I). In the later set of plots (H, F, G, I), if H plot was indeed the coarser, the specific structure of the other plots did not lead to the same plots rank by all the structural parameters. For example, G Plot was similar to the F plot in term of total density, but was closer to the H plot when considering only trees greater

than 30 cm dbh. Also, with its low density but high relative number of trees greater than 30 cm dbh, the I plot obtain a higher mean tree diameter than the F plot even though its AGB is estimated to be about 100 t. DM. ha<sup>-1</sup> lower. It is noteworthy that plots K, J, and to a lesser extent, I, greatly differ from the other plots in term of species composition and structural features. Indeed, these plots underwent an intense fire about two decades ago which led to the formation of a secondary succession composed of pioneer (e.g. *Acacia sp.*) and sparse deciduous species while other plots were located in undisturbed mature evergreen stands. Plots K and J were characterized by a very low understorey with more than 80% of trees in or higher than the canopy strata while this proportion falls below 60% in undisturbed plots (i.e. G and P; Fig. 26).

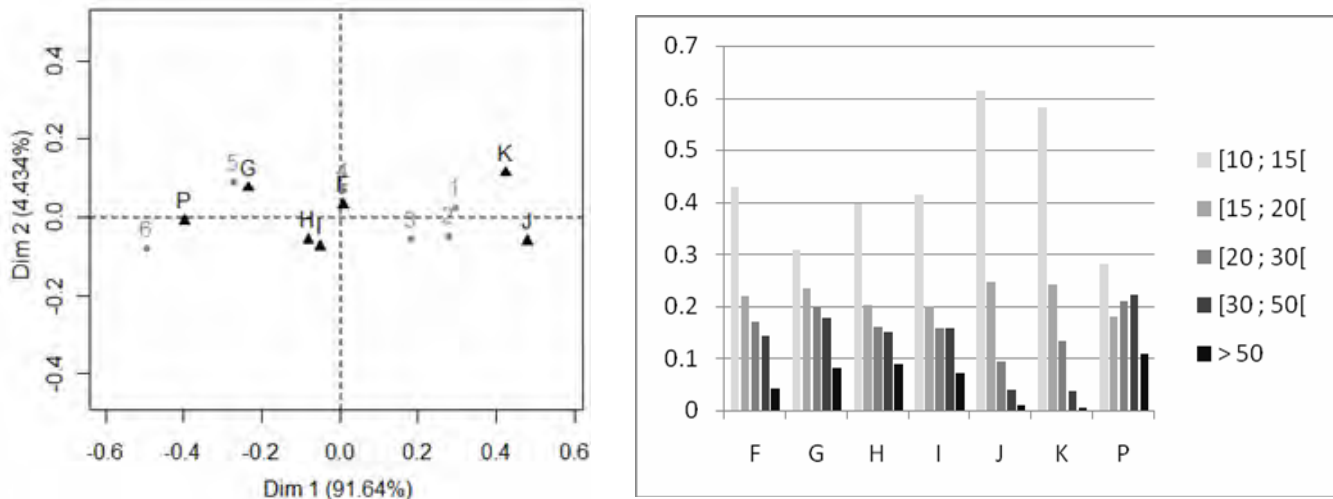


Figure 27. (left) First plan of CA on 6 equal-count dbh bins (only CA1 is used later on the analysis); (right) Distribution of relative frequencies (%) on 5 dbh bins among plots.

### 3.4.2. Model calibration

Windows covering the ground plots (see methodology) were added up to the PCA data as supplementary individuals and the barycenters of their coordinates along PCA axis 1 (model 1) and PCA axes 1 and 2 (model 2) were used as indexes of canopy texture. Figure 28 shows that even though modeled forested scenes (DART) obtained very similar positions along PCA1 in the IKONOS and GE-derived factorial plans, this is not the case for real forested scenes.

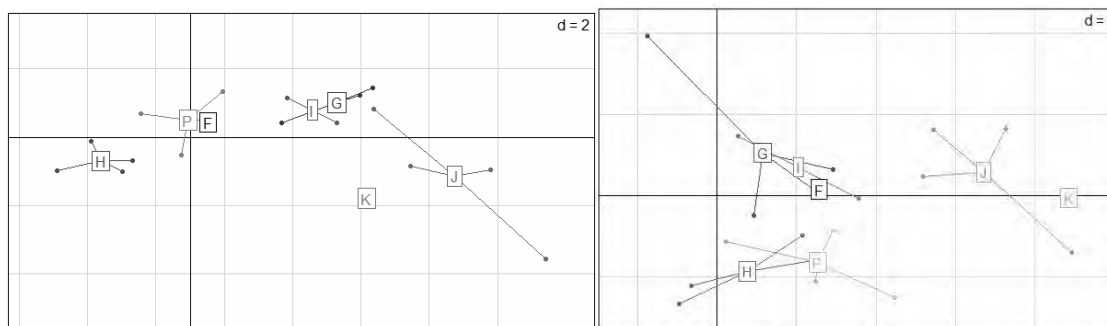


Figure 28. Ground plot position on IKONOS-derived (left) and Google Earth-derived (right) factorial plans (grid mesh = 2)

Several observations can be made from the above figure. There is a higher variance among windows constituting each plot on the GE-derived factorial plan, which underline greater differences in the range of dominant spatial frequencies that characterize each, although overlapping, windows. This observation confirms the higher quality of the IKONOS-derived textural indice. Secondly, the displacement of plots barycenter from IKONOS-PCA1 to GE-PCA1 does not always occur in the same direction and globally result in a grouping of the coarse with the intermediate canopy grains plots on the positive side of GE-PCA1 close by the origin. This could imply a form of saturation of the GE-derived textural gradient in its discrimination of windows canopy grain, but remains surprising given the good ordination of DART scenes all along the PCA1 gradient. The poor relative position of the plots on PCA1, particularly the coarse canopy-grain H and P plots, may be explained by their own textural specificities combined with the lower spatial resolution of GE image. Fig 28 indeed show that both plots scores higher than the entire window set for spatial frequencies above 170 cycles.km<sup>-1</sup> ( $\lambda < 6$  m) in the GE image only, which explain their steering toward the positive side of PCA1.

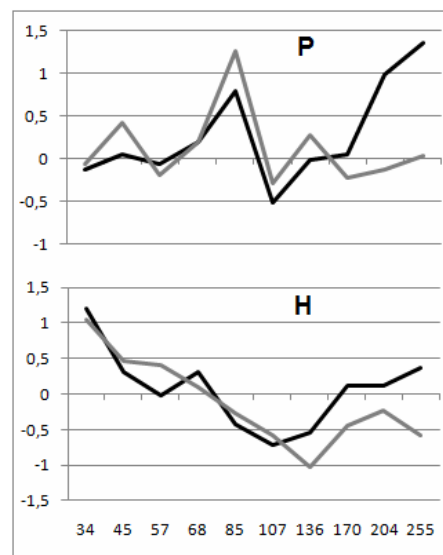


Figure 29. Plots P and H standardized r-spectra derived from IKONOS

Simple linear regressions and linear models were carried out to test the explanatory power of the canopy texture indexes regarding ground-plots structural parameters. Regressions quality was characterized with the adjusted coefficient of determination ( $R^2$ ), the root mean square error (rmse) expressed in arithmetic units and the relative error (s) in percent. The following figures illustrate the results based on the first PCA axis only and derived from IKONOS (Fig. 30) and GE (Fig. 31).

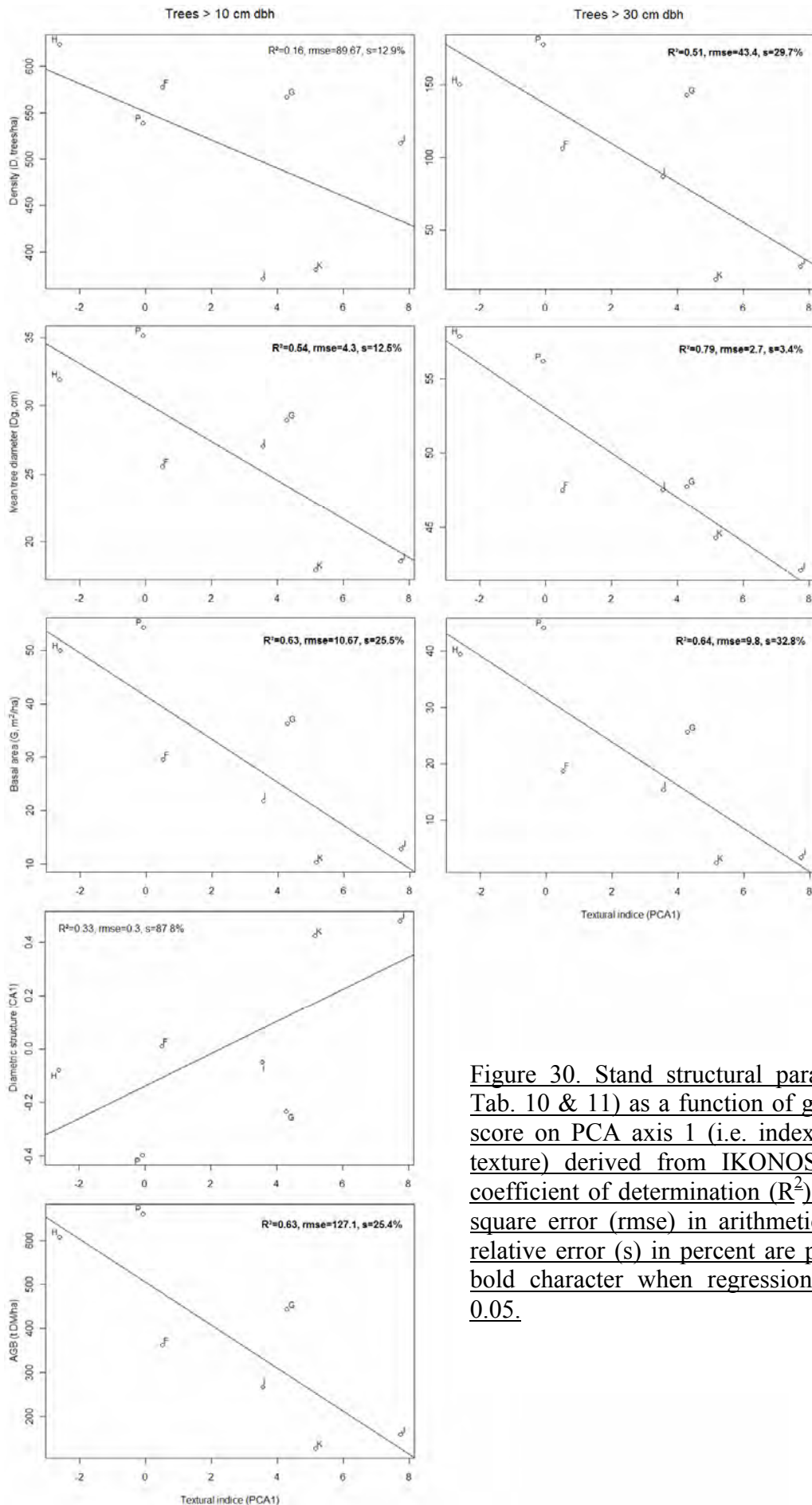


Figure 30. Stand structural parameter (see Tab. 10 & 11) as a function of ground plots score on PCA axis 1 (i.e. index of canopy texture) derived from IKONOS. Adjusted coefficient of determination ( $R^2$ ), root mean square error (rmse) in arithmetic units and relative error (s) in percent are presented in bold character when regression p-value < 0.05.

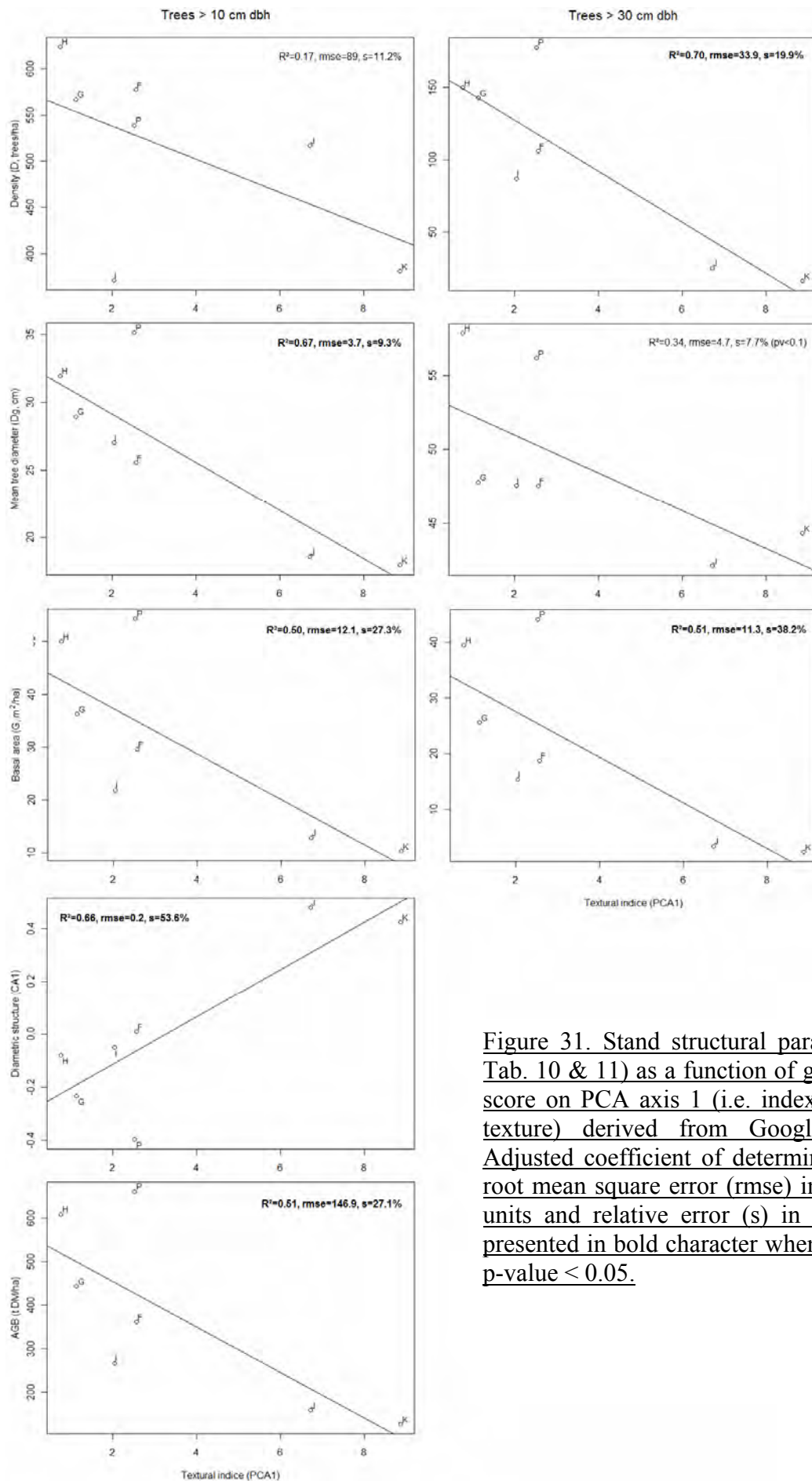


Figure 31. Stand structural parameter (see Tab. 10 & 11) as a function of ground plots score on PCA axis 1 (i.e. index of canopy texture) derived from Google Earth™. Adjusted coefficient of determination ( $R^2$ ), root mean square error (rmse) in arithmetic units and relative error (s) in percent are presented in bold character when regression p-value < 0.05.

The first axis of the IKONOS-derived factorial plan was good predictor of mean tree diameter (Dg) with an  $R^2$  above 50% and a low relative error ( $s = 12.5\%$ ). This axis also reasonably predict stand basal area and AGB estimate with fairly similar  $R^2$  but higher relative errors ( $s = 25\%$ ). Total stand density (D) or stand diametric distribution (CA1) did not led to significant relationship with the textural index but considering only trees greater than 30 cm dbh led to significant relationship with stand density ( $R^2=0.51$ ,  $rmse=43.4$ ,  $s=29.7\%$ ) and increased the predictive power on Dg.

The linear model involving both PCA axes as predictor variables for stand parameters did not led to a significant contribution of the second axis, except for the prediction of stand diametric distribution ( $R^2=0.80$ ,  $p\text{-value} < 0.05$ ,  $rmse=0.146$ ,  $s=37.2\%$ ). Lets note however that other models yield a second axis significant at 0.1, with Dg and  $D^{>30\text{ cm dbh}}$  as response variables, increasing the fit of the models ( $R^2$  of 0.74 and 0.75) and lowering the relative error ( $s$  of 7.3% and 20.9% respectively).

The GE-derived FOTO index based on PCA1 obtain similar prediction trends on stand structural parameters as the IKONOS-derived one. Good predictions were obtain with Dg ( $R^2=0.67$ ,  $rmse=3.7$ ,  $s=9.3\%$ ), G ( $R^2=0.50$ ,  $rmse=12.1$ ,  $s=27.3\%$ ) and AGB estimates ( $R^2=0.51$ ,  $rmse=43.4$ ,  $s=29.7\%$ ). Once we considered only the subset of trees greater than 30 cm dbh, the GE-derived FOTO index was also a significant predictor of tree density ( $R^2=0.70$ ,  $rmse=33.9$ ,  $s=19.9\%$ ), but it did not improve the relationship with Dg.

Unlike in the case of IKONOS, the 2<sup>nd</sup> GE-derived PCA axis significantly contributed to stand structural parameters predictions. However, the marked differences between windows ordination along GE and IKONOS-derived 2<sup>nd</sup> axes stress the need to take these results with caution. The linear model resulted in improved relationships with AGB estimates ( $R^2=0.84$ ,  $rmse=82.7$ ,  $s=13.5\%$ ), basal area for all trees G ( $R^2=0.84$ ,  $rmse=6.8$ ,  $s=13.5\%$ ) and trees greater than 30 cm dbh ( $R^2=0.86$ ,  $rmse=6$ ,  $s=18\%$ ) as well as their mean diameter  $Dg^{>30\text{ cm dbh}}$  ( $R^2=0.96$ ,  $rmse=1.1$ ,  $s=1.5\%$ ).

### 3.4.3. Model inversion

We re-computed the textural clusters defined earlier (see 3.1 Textural analysis) to take into account windows displacement induced by the partitioned standardization technique and used these clusters to map the canopy texture over the study area (Fig. 32). Stand structural parameters that led to the best relationships with the textural indices are predicted per textural cluster (Tab. 12).

Table 12. Structural parameter predictions inferred from the above regressions and based on IKONOS image. Mean and SD values per cluster of canopy texture.

Predicted variables	model			Clusters of canopy texture				
	a <sub>0</sub>	a <sub>1</sub>	a <sub>2</sub>	C1	C2	C3	C4	C5
D <sup>&gt;30cm dbh</sup> (trees h <sup>-1</sup> )	133.6	-11.0	29.3	168.6 (37.4)	160.6 (34.9)	140.3 (34.6)	98.8 (34.8)	31.4 (21.1)
Dg (cm)	29.9	-1.2	2.8	34.0 (3.6)	32.7 (3.5)	30.5 (3.3)	26.2 (3.4)	16.2 (4.4)
G (m <sup>2</sup> ha <sup>-1</sup> )	41.5	-4.0		63.6 (5.4)	50.1 (3.3)	39.5 (3.2)	27.4 (4.0)	13.7 (5.6)
AGB (t. DM. ha <sup>-1</sup> )	505.3	-49.0		772.7 (65.9)	609.1 (40.1)	480.8 (38.4)	334.8 (48.4)	167.9 (68.4)

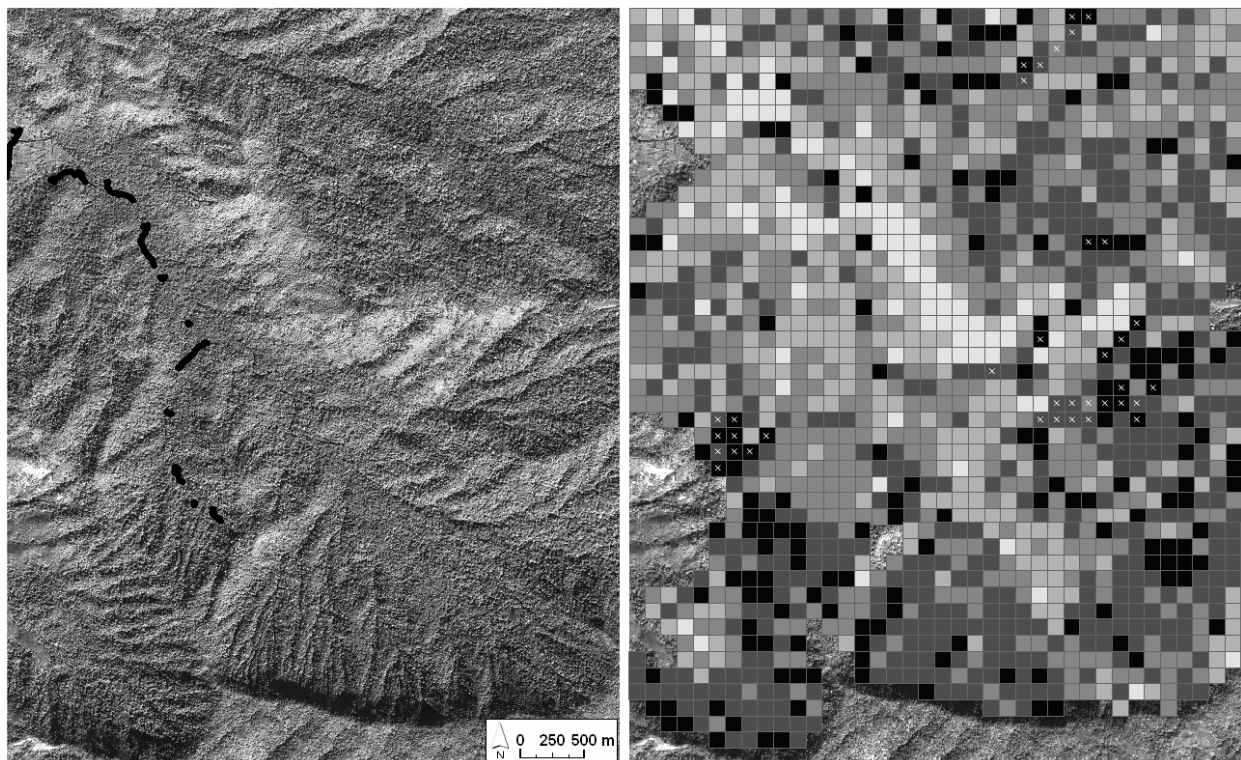


Figure 32. (left) Project study area, near to Uppangala village (Western Ghats, India) – black dots represent a GPS trace along the trail road crossing the area; (right) same area overlaid by 125 m side square windows with grayscale corresponding to the canopy texture clusters defined previously (see Fig. x-c (plan PCA) and Tab. X), from black (cluster 1, very coarse canopy grain) to light gray (very fine canopy grain). In the top 19 km<sup>2</sup> (i.e. GE image extent), white crosses represent windows particularly marked by relief-induced illumination discrepancies, resulting in a poor canopy characterization.

Both stand parameters predicted with the model involving the 2 firsts PCA axes display overlapping ranges of predicted values across the four first textural clusters. The overlapping proportion is particularly marked between the two firsts' clusters and then decrease toward the 4<sup>th</sup> cluster. This drawback is induced by the very use of the second axis combined with a poor model calibration in the coarse-grain edge of the textural gradient. Indeed, the ground-plots positions in the PCA observations cloud do not cover the decrease of windows ordination along the second axis toward coarse canopy grain and therefore results in a strong positive model coefficient for A2 (i.e.  $a_2$ , Tab. 12). Because of the horseshoe-shape of the PCA cloud (i.e. C1 more negative on PCA1 and PCA2 than C2), the two model coefficients of contrary signs (i.e.  $a_1$  and  $a_2$ ) tend to compensate themselves while predicting stand parameter values, which results in this lack of clear differences between clusters. Such drawback is logically not observed on the predictions of G and AGB, which are linearly derived from one PCA axis only.

The spatial distribution of textural clusters over the study area (Fig. 32) is consistent with the forests structural variations observed on the field. The general pattern display a coarser canopy grain the less the stand is accessible, which may be explain by different degrees of anthropological disturbances throughout time. The Uppangala village is roughly located nearby the North-West corner of the area, and a trail road cross the area from this corner to the West bottom of the fully illuminated hills observable in the satellite image (Fig. 31, left) down to the bottom of the major hills located on the South of the area. We can indeed see that the finest canopy structures are mainly found on the North-West quarter of the area, close to the village, along and around the trail road, while the canopy grain become coarser away from this "frequented" part, the further the terrain display steep slopes and abrupt elevation variations.

We can also notice that most of the very fine texture (i.e. lightest gray color) is found on these fully sun-lighted hills that form a diagonal band on the study area top part, while most of the very coarse texture (i.e. near-black color) are found on stands containing marked topographical features (e.g. thalwegs) and in turn marked illumination patterns within the unit-window. Even though it has been noticed on the field that e.g. very fine canopy grain were found on the fully illuminated hills, the former observation raises the question of the extent to which the partitioned standardization correct for topography-induced biases in the canopy texture characterization.

## 4. Discussion

### 4.1. Google Earth™ images performances

We assessed Google Earth™ image performance as input for the FOTO method by comparing the canopy textural gradient (i.e. FOTO index) derived from the former image type to the one derived from IKONOS™ image, the GE native image considered as a reference.

#### 4.1.1. Set up and limits

Lets first bear in mind that the main differences existing between the two image types are the spectral information (IKONOS panchromatic grayscale against GE average of RGB true color bands) , spatial resolution (metric IKONOS resolution against the coarser and unknown GE resolution, considered to be about 2 m.pixel<sup>-1</sup>), unknown additional radiometric and geometric corrections applied to GE images and lastly, an increased positional error of GE images estimated to range from 2 to 115 m in Western and South-central Asia (Potere, 2008). As underlined by Barbier (2009), the FOTO method presents the advantage of being relatively independent from the absolute values of both the mean and variance of the image, because the mean-centered images are characterized by the proportion of variance explained by spatial frequency bins. It follows that differences in images contrast or luminosity should not influence the results as long as the spatial arrangement of relative pixel values is conserved. If the positional error induced by GE do not modify the spatial arrangement of features (Montesano *et al.*, 2009) and should therefore not bias the FOTO results (model calibration/validation issues apart), it hinders our IKONOS-GE comparison. Indeed, the small positional difference between IKONOS and GE images results in small differences of ground area covered by each “fix” unit-window and therefore induce variability in the resulting FOTO index per unit-window which bias window to window direct comparison. Moreover, the PCA axes of IKONOS and GE-derived factorial plans being computed on the basis of the total image variances, which differ among the two image types, a co-inertia analysis should have provided more reliable results than direct comparison of ordination scores. However, our rough and straight approach consisting of a direct comparison of unit-window scores along PCA axes of both factorial plans reveal trend differences in window relative position that may orientate further researches.

#### 4.1.2. Textural gradients

##### *A certain extent of similarity*

We initially observed that the r-spectra variability among unit-windows of the two image types was decomposed in a fairly similar way by the PCA technique. In both cases the two first axes were retained. The largely prominent first axes explain about 40% of the total variances and compose the core coarseness-finesse textural gradient, while the second axes only counted for 7 % (IKONOS) and 10 % (GE) of the variances and were considered to carry information on window texture homogeneity, a potentially interesting feature of stands structural organization. This first analysis step provides comparable results to previous FOTO applications based on GE images (PCA1: 48%, PCA2: 9%, Barbier *et al.*, 2009) and, to a lesser extent, IKONOS panchromatic images (PCA1: 58%, PCA2: 13%, Proisy and al., 2007). In the later case, the authors were studying mangroves forests of French Guiana. Those forests are composed of very few species, display a limited number of development stage trajectories and present a relatively high stand homogeneity (e.g. tree age) due to major environmental constraints (Fromard *et al.*, 2004), which should simplify the range of periodic textural patterns detectable by FOTO and result in heavier PCA axes (less noise).

It is also interesting to note that in the framework of the later study, FOTO results based on IKONOS 1 m panchromatic image and IKONOS 4 m NIR channel were compared and yield distinct organizations of the different mangrove development stages on the two firsts PCA axes. Such difference has not been observed in this study, IKONOS and GE images led to PCA observation clouds of fairly similar shape and extent without obvious differences in window canopy grain organization. Direct comparison of windows positions along IKONOS and GE-based PCA axes however allowed us to glimpse the main differences between the derivable textural indexes. The two major textural gradients (i.e. GE and IKONOS PCA1) were fairly consistent ( $R^2= 50\%$ ,  $rmse=2.5$ ) with increasing differences at both edges of the gradients. A limited part of the window set was concerned by important displacement from one factorial plan to the other and largely contributed to weaker the relationship between the two axes. Interestingly, the promising match between the two main and major axes (i.e. PCA1) was supported by very similar DART scenes positions, which show that IKONOS and GE windows sets' variance in term of r-spectra distribution over spatial frequencies yield to the computation of a very similar main PCA axis, allowing the consistent ordination of noise-free simulated supplementary scenes. Windows' ordination along the second PCA axes was however prone to a greater variability with an  $R^2$  value as low as 5%. Besides, the analysis of topographical variables influences over PCA axes shown that if GE-PCA1 displayed the same though weaker trends of sensitivity than IKONOS-PCA1, such similarity was not found between the second PCA axes which exhibited distinct relationships with the different variables. Notably, GE-PCA2 was not significantly influence by window aspect or slope-aspect combination and weakly with the main hillshade variable ( $R^2=2\%$ ). The axis was surprisingly well correlated to window mean elevation ( $R^2=22\%$ ) unlike IKONOS-PCA2 ( $R^2=2\%$ ) which may point toward an effect/artifact induced by GE geometric corrections.

Although the relative position of ground-truth plots differs among the two factorial plans, GE-PCA1 was a significant predictor of several stand structure parameters with a comparable and sometime slightly better fit to the observed data than IKONOS-PCA1. Surprisingly, despite its marked differences with IKONOS-PCA2 and unlike the latter, GE-PCA2 significantly contribute to stand parameters predictions and increase the models accuracy such as with mean basal area ( $R^2=0,84$ ) or the AGB estimate ( $R^2=0,84$ ). Let's also underline that if GE-derived FOTO indexes yield good regression scores with stand structure parameters, they present a major flaw due to the relative position of ground-truth plots in the canopy textural gradient, notably on PCA1. In the case of the PCA1-based model for example, the coarser plots being located at an intermediate position on PCA1 and stand parameters being linearly linked to windows ordination score, the model predict unrealistic parameters values for windows located on the negative edge of the axis (e.g. intercept of AGB prediction model above 500 t. DM.ha<sup>-1</sup>). Such flaw is also observed with IKONOS images but to a lesser extent.

These results confirm the potential of GE images to characterize forest canopy structure but stress the need for further investigations. A better understanding of GE image characteristics influences on the observed differences of forest scenes relative positions along PCA axes compared to the IKONOS reference should help minimize this variability and accurate GE-based FOTO results.

### *Dissimilarities and research avenues*

It remains difficult to explain the differences in ordination scores of real forested scenes along PCA axes of the two factorial plans, because of the multiples differences between image types, notably in terms of spatial resolution and spectral information. The sensibility of FOTO to image spatial resolution as well as the effect of this instrumental parameter on canopy r-spectra have not been specifically addressed so far and could be investigated with a modeling approach (e.g. DART model). The small value range of GE averaged bands (Fig. 18) is also one pitfall that should certainly contribute to the observed differences with IKONOS, and one should attempt to optimize this range with more a complex combination of the RGB bands.

This decrease in tonal variations combined with the coarser spatial resolution of GE hinder the visual recognition of individual crowns limits and may have a specific effect on window r-spectra computation according to stand canopy structure and its spatial organization within the unit-window. Although the window set exhibit a great variability of canopy structure (tree density, crown size distribution, etc) and possible spatial arrangements, preventing any straight and simple relationship between stand structural features and the observed differences' trends between GE and IKONOS results, one could advance the following hypotheses: on the coarser spectral and spatial resolutions image type (i.e. GE), the largest and more pronounced canopy patterns or shaded areas visually remains and represents a greater share of image variance than on the higher resolutions image (i.e. IKONOS) because of the decrease or disappearance of fine scale variations (spatial and spectral). For the later reason, the presence and spatial arrangement of such marked features seems to play a greater role in window r-spectra computation for the lower resolutions image type. An heterogeneous stand structure (tree height notably) with marked emergent trees and/or canopy gaps often display spatially heterogeneous shades of large size (i.e. induced by the differences in tree height or canopy gaps ; Fig. 17 - right) and may therefore be overestimated (i.e. considered as coarser, higher proportion of image variance accounted for low spatial frequencies) by the low resolutions images, while the r-spectra of the same window captured in high resolution imagery may be balanced by a greater relative detection of smaller and less clearly marked patterns (crown limits). On the other hand, dense, homogeneous forest stands are less subject to such spatial heterogeneity (closed canopy, homogeneity in tree height), display more periodic tree shade patterning (Fig. 17 - left) and should therefore be less influenced by this potential bias. This trend seems also confirmed with the largest patterns, in terms of macro-heterogeneity or –homogeneity (Fig. 33), which support that GE-PCA1 might be more sensible to texture homogeneity than IKONOS-PCA1.

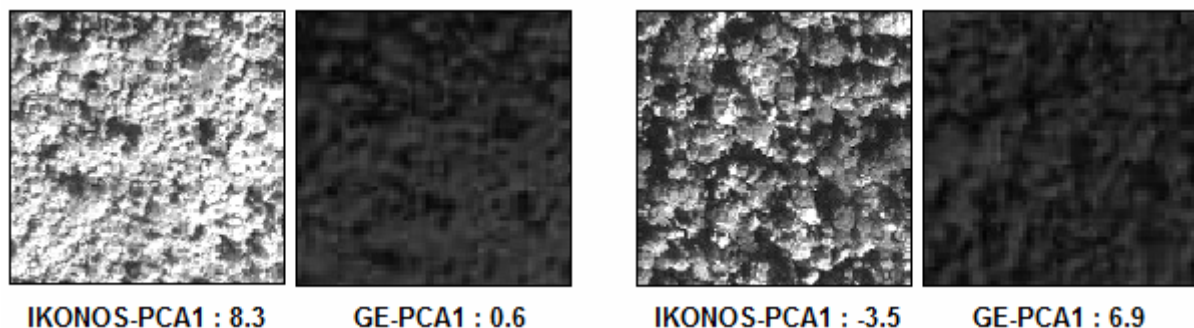


Figure 33. The two scenes on the left display a macro-heterogeneity, with tree shades gradually more pronounced from the bottom-right to the top-left corner. Such scenes seem particularly overestimated by GE. The two scenes on the right display a particular macro-homogeneity with periodic and rather homogeneous tree shades. Such scenes seem particularly underestimated by GE.

The influence of spatial heterogeneity on window ordinations may be investigated by coupling the FOTO method to e.g. a lacunarity analysis. Lacunarity is another form of textural analysis particularly relevant to characterize image spatial heterogeneity at diverse scales. Frazer *et al.* (2005) shown that such analysis allowed to accurately characterize stands canopy according to canopy cover and intercrown gap volume, an example of “spatial heterogeneity” index that may provide new insights into FOTO windows classification.

#### ***4.1.3. Interest and remarks***

It is likely that GE images characteristics (spatial and spectral) as well as the extent of Earth coverage underlaid by high resolution images will increase in the coming years, which make pertinent to investigate the potential of this virtual globe software for forest research studies. This free-access database provide the opportunity to collect quality satellite data at spatial scales (e.g. regional) that would not be economically conceivable for research studies relying on commercial products such as hyperspatial IKONOS images (10x10km). Latest researches in the field of tropical forest mapping have indeed succeed to value GE database, in combination with affordable level of commercial data (i.e. Lidar), to assess forest carbon distribution over extensive areas (above 4,000,000 ha; CLASlite Peru REDD demo) and for a limited cost (about \$0,10 USD.ha<sup>-1</sup>) while maintaining a high spatial resolution (30m) and accuracy (10%) (CLASlite Haway REDD demo; Asner *et al.*, 2009a). It is however unclear whether the latter results were based on GE native images provided by Google <sup>TM</sup> or images extracted from the GE software, similarly to the present approach. Our results suggest that GE images directly extracted from the software provide a sufficient level of information for FOTO to discriminate windows on the basis of canopy textural patterns that indeed significantly relate to a certain number of stand biophysical attributes. The quality of the GE-derived textural gradient was however poorly assessed because of the limited number of sample plots leading to a poor model calibration and the absence of model validation step. These results are nonetheless promising and should lead to further research notably to disentangle the influence of spatial and “spectral” image resolutions on FOTO, and in turn increase our understanding of GE images potential and limits.

For FOTO to be operational, notably with GE images, it would also worth investigating the method sensibility to sample plots geo-location error. This common remote sensing-related source of uncertainty constrained us to extract 4 overlapping windows per sample plot, which shown a certain extent of variability once positioned on the FOTO textural gradient, particularly marked with GE images. This uncertainty, hampering an accurate mode calibration, may be quantified with simple statistical techniques (Anser *et al.*, 2009b) to compute prediction confidence interval.

#### ***4.2. Relief variations***

The project study site being topographically diverse, it was necessary to identify and attempt to correct for potential influences of relief variations on the FOTO-derived textural index. Our analysis suggest that image texture variations related to topography indeed influence unit-window r-spectra, at different spatial scales, which in turn alter the reliability of the derived canopy textural index.

#### **4.2.1. Contribution to windows macro-heterogeneity**

A first and obvious influence of topography variations on window r-spectra was identified in the first steps of the textural analysis by comparing window position on the PCA plan to the visual assessment of canopy grain-size it contains. We have shown that unit-windows overlaying a ridge or a valley bottom could encompass two distinct types of canopy texture, due to underlying abrupt terrain variations, and were therefore characterized by a marked macro-heterogeneity. Those windows were positioned in the textural gradient regarding this heterogeneity rather their specific canopy grain, preventing an accurate inferring of their biophysical characteristics. These results partly confirm the observations of Coueron *et al.* (2005) who explained windows loading on the 2<sup>nd</sup> PCA axis by this relief-induced macro-heterogeneity. In the latter study, windows subjected to this macro-heterogeneity seemed indeed to be consistently positioned along the PCA1 while obtaining high score on the second axis. We may explain the stronger effect observed in our analysis (i.e. macro-heterogeneity influence on PCA1) by the selection of a larger window size (125 m against 100 m) or more pronounced relief variations.

Although this macro-heterogeneity profoundly influence window r-spectra and relative position in the textural gradient, it affects a limited number of windows (< 5% in our case) and therefore do not induce major bias in the PCA axes (un-presented results). Lets however note that we quantified this window subset by a subjective visual assessment and may have left apart windows affected by this bias to a lesser extent. Attempts to automatically select those windows on the basis of DEM data (hillshade range or SD, presence of large TIN-polygons of opposed aspects, etc.) proved difficult. Mitigating this source of noise may be achievable by selecting smaller window sizes, or through pixel-based radiometric corrections.

#### **4.2.2. Influence on canopy textural patterns**

Our results also emphasize more global influence of topography variations on window r-spectra, consistently with working hypothesis that could has been formulated from the literature. It has been indeed stated that on slopes facing the sun, forest canopy appear brighter to the sensor since at finer scale, a larger proportion of each tree crown is illuminated, and the other way around on slope facing away to the sun. This variation in the crown-shade sizes relationship lead to different image textures for similar forest stand and must be normalized to compare windows on the same bases.

It was first necessary to attribute to each unit-window an index value characterizing the effect of relief variations on canopy illumination, in order to identify the influence of this effect on window ordination and gather unit-windows with homogeneous index values. Both types of spatial variables (i.e. manually computed and hillshade) depicted the same significant trends although the hillshade model captured a greater share of variability. Linear regressions (hillshade) and multiple means comparison tests (manually computed variables) confirmed that on slopes facing the sun, windows tend to be ordinated toward the positive side of PCA1 (i.e. fine canopy-grain) while windows facing away to the sun tend to be ordinated toward the negative side of the axis (i.e. coarse canopy-grain). Spectral analysis indeed showed that the brightest windows group is characterized by a significant higher dominance of small patterns (< 11m) and a lower share of image variance explained by large patterns compared to the darkest one and regardless of the canopy grain size. We can therefore state that for a given stand, variations in proportion of sun-lighted and shaded tree crown driven by slope's aspect regarding the sun position bias window ordination toward coarser or finer canopy grains. This relationship was marked on the second half of e.g. the hillshade gradient (illuminated part) and seems to disappear on the first half that relate to windows particularly shadowed by relief

variations. This result seems consistent because on windows strongly shaded by their geomorphologic set up and the surrounding environment, trees may only be illuminated by diffuse and scattered lights rather than direct sun light, and therefore do not display shade.

A simple partitioned standardization with as few as 4 hillshade bins allowed removing the unwanted influence of the hillshade on both PCA axes. It also factored out the significant though weaker influences of spatial variables manually computed, which support the potential of this hillshade model to correct for topography-induced biases. The hillshade function is easily and rapidly computable with GIS software such as ArcGis and could be integrated to the FOTO routines. Further investigations suggest that partitioned coordinates do not increase the fit of the FOTO index to stand structural parameters (see Appendix 5) and it would therefore be interesting to assess the effect of this correction on the accuracy of stand parameter predictions with the appropriate study design (ground plots across a gradient of hillshade).

Let's finally note that the influences of elevation variables on PCA1 were mitigated but still significant, notably with the mean window elevation ( $R^2=0.035^*$ ), which could point toward a actual effect of elevation on forest structural organization. Few studies have documented tropical forest structure and AGB spatial changes with altitude and those parameters vary greatly among tropical forest types (Wang *et al.*, 2006), even at the same altitude (Austin *et al.*, 1972, in Aiba and Kitayama, 1999). It arises from the literature that altitudinal gradients modify forest structure through changes and complex interactions among and between abiotic (temperature, rainfall and humidity, substrate nature and nutrient availability, wind) and biotic factors. It is commonly observed that stem density increase with elevation (Wang *et al.*, 2006; Aiba and Kitayama, 1999; Lieberman *et al.*, 1996) while tree height, dbh and AGB estimate decrease (Wang *et al.*, 2006; Miyajima and Takahashi, 2007; Aiba and Kitayama, 1999; Asner *et al.*, 2009c), which contradicts our findings on the Ghats that show a slight decreasing trend in window ordination along PCA1 (i.e. coarser canopy-grain) with elevation, and therefore an increase in e.g. AGB estimate. This difference might first be explained by the ranges of elevation in consideration. Elevation on our study site range from 200 to 1100 m, which is fairly below most of the high elevation range limits found in the literature (up to 3100 a.s.l., Aiba and Kitayama, 1999). Lieberman *et al.* (1996) also obtained contrasting results along a large altitudinal gradient (30 to 2600 m) of Costa-Rican tropical forest with a constant mean tree diameter from 30 to 1500 m a.s.l. which slightly increased at higher altitudes and greater mean basal area on the highest plots. One should also take into account the influence of local topography (slope, aspect) on forest structure organization, which proved to dominate altitudinal influence on several stand structural parameters (D, Dg, mean tree height; Wang *et al.*, 2006). Considering this effect is relevant in our study area, because most of the elevation increase is concentrated in the southern part of the site which therefore display steep slopes and North, North-West, West main aspects. For example, forest stands growing on slopy terrain are known to be denser and smaller in height and mean trunk diameter (Wang *et al.*, 2006) due to e.g. mechanical constraints or better access to light. Nevertheless, there are also contrasting observations with for example, Hartshorn and Peralta (1988, in Lieberman *et al.*, 1996) whom documented denser but taller stands on sloping landforms, which was attributed to a better soil drainage. The variability of elevation and local topography influences on forest structure stress the importance of local site conditions (e.g. soil quality) and support a possible increase of forest canopy grain size with elevation on the study area, which would be consistent with field observations but could also be partly induced by a bias of the method (see : next part). Last but not the least, anthropogenic disturbances on low elevation – more accessible areas may have contributed to the observed trend.

### ***4.3. Characterization of tropical forest canopy structure***

This first assessment of the potential of the FOTO method to characterize the wet evergreen forests of central Western Ghats provided consistent results with respect to previous FOTO applications. Our empirical findings indeed confirm that similarly to the mangrove (Proisy *et al.*, 2007) and lowland evergreen rain forests (Couteron *et al.*, 2005), canopy images of wet evergreen forests display pseudo-periodic patterns leading to the dominance of specific spatial frequency ranges in window r-spectra that allow characterizing and discriminating forest types. It is however apparent that at the current methodological development stage, environmental variables (local topography) and forest structural complexity modulate FOTO results precision and accuracy.

#### ***4.3.1. Several scales of spatial heterogeneity***

On the basis of previous FOTO applications, and notably the results of Proisy (2007) on the mangrove forests of French Guiana, we emphasized the influence of image spatial heterogeneity on the performance of FOTO. Spatial heterogeneity arises at several scales and is induced by diverse factors.

Our study area presents the specificity of being topographically diverse, and we shown that local geomorphology could create large illumination patterns on forest canopy that account for most of the image variance and therefore strongly bias window ordination toward these large patterns. Topography variations also induce a weaker and more subtle bias, not directly induced by local geomorphology but rather its effect on forest structure. It is well known that canopy gaps and chablis/tree falls are more abundant on sloppy terrains than on flat grounds, because of decreased tree stability (mechanical constraint), increase exposition of tree crown to the wind, etc. This natural disturbance trend has been observed on the study area (Pélissier, 1998) and should be more pronounced as elevation increases, because distances between thalwegs often decrease as we get closer to hill tops, which results in a greater frequency of thalwegs – interfluves terrain variations. Within the unit-window, canopy gaps and medium to large tree falls create a spatial heterogeneity fairly well detected by varying low spatial frequencies (depending on their spatial arrangement) and therefore contribute to a certain extent to bias window ordination toward coarser canopy grains. This element may contribute to the remaining influence of elevation on PCA1 after the partitioned standardization technique which was not designed to correct for such bias. Beside the direct and indirect influences of land forms on the textural index, the spatial heterogeneity displayed by complex tropical forest canopies may also hamper the classification process.

Spatial patterns and structure of the outer forest canopy are commonly described to vary with the size, shape, abundance and spatial arrangement of canopy trees as well as the inter- and intra-crowns gaps of varying sizes (Frazer *et al.*, 2005). Although we have a limited understanding of the physical and biological determinants of forest canopy pseudo-periodicity, it seems logical to think that the more structurally and spatially (horizontal and vertical) diverse is this canopy layer, the less pseudo-periodic it gets. For instance, forests compose of very few canopy species such as mangrove forests of French Guiana should display fewer variations in e.g. crowns geometry and sizes amplitude than hyper-diverse wet evergreen forests, and therefore display a greater periodicity. Similarly, the great spatial homogeneity of mangrove forests in tree height and allometrically related parameters contribute to image texture homogeneity/patterns periodicity and minimize the spurious effect of spatial heterogeneity on window r-spectra. Such homogeneity in age/height at the unit-window scale is less often encountered on the pluri-strata wet tropical forests of the Central Western Ghats (CWG) that often display a certain extent of macro- and meso- heterogeneity

throughout successional stages. For example, the post-fire highly degraded secondary successions notably display tall emergent trees that survived the fire, patches of shrubs of varying sizes or variations in re-growth crown sizes that may relate to local site conditions (e.g. soil depth variations along the slope). In the other side of our textural gradient, mature – primary wet evergreen forests are also characterized by the high occurrence of the large emergent trees that shade the canopy as well as gap openings and crown aggregations that contribute to create a meso-scale spatial heterogeneity in the image. It follows that spatial heterogeneity has a much greater influence on windows r-spectra of upland wet evergreen forests than on mangrove forests (fig 34.)

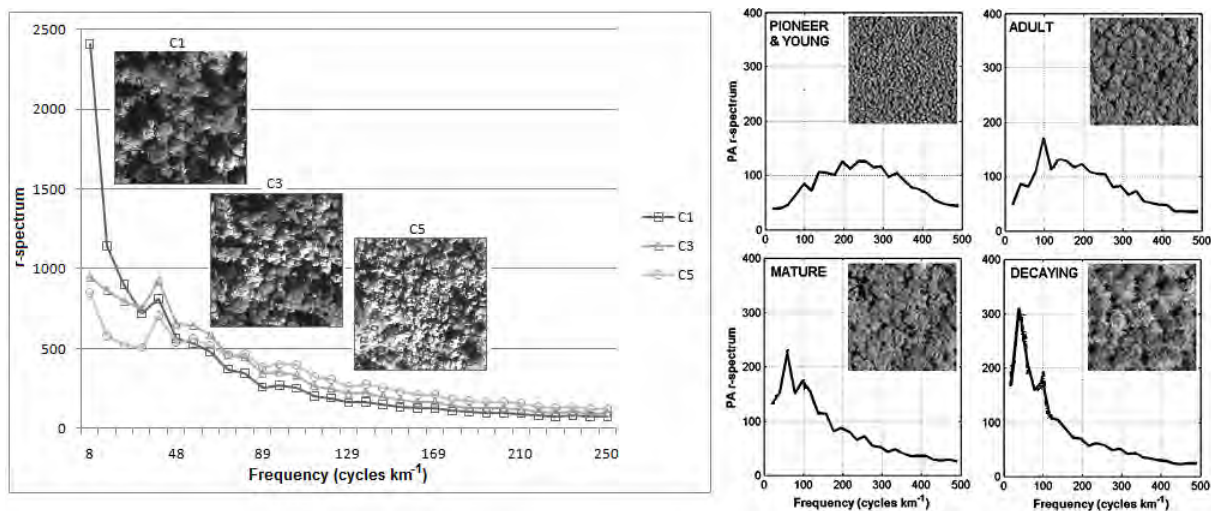


Figure 34. Averaged r-spectra per cluster of canopy texture on (left) wet evergreen forest of the CWG (window size: 125m) and (right) mangrove forests of French Guiana (window size: 100 m; from Proisy et al., 2007).

While obvious differences can be visually observed among averaged r-spectra of mangrove development stage clusters, this is not the case with the wet forests of the CWG. The mean of textural clusters raw r-spectra are always skewed toward low frequencies, even in the case of fine texture (C5), and our stand discrimination is therefore based on much smaller differences / specificities of each cluster mean r-spectra. This is of course a major obstacle in our study and more broadly, for the application of FOTO on structurally complex hyper-diverse tropical forests. Mitigating this bias should be achievable by using smaller window sizes (< 125 m).

#### 4.3.2. Ability of FOTO to discriminate forest structure in our case study

##### Limits

Although the calibration of the FOTO-derived canopy textural gradient with modeled stands (DART) yield a very good linear fit of several stand structural parameters on the basis of PCA1 only (e.g.  $R^2 = 0.85$  for mean tree dbh) or both PCA axes (e.g.  $R^2 = 0.97$  for mean tree dbh), we obtained weaker relationships with our set of real stands images. This second calibration was indeed weakened by several factors, primarily the insufficient number of sample plots and failure to cover the entire gradient, particularly along the negative side of PCA1 (i.e. coarse grain). The intermediate positions of plots along PCA2 also hamper the proper calibration of this axis and stress the importance a field work that should specifically target plots located on the most homogeneous canopy grain conditions. This poor model calibration notably result in a great within-cluster variability in predicted structural parameters and is the primary factor to be improved during further applications of the method on this study area.

### *FOTO index and canopy structure*

The relationships between FOTO canopy textural index and stand structural parameters on the wet forests of the Ghats mostly differ from the ones established on the lowland evergreen rain forest of French Guiana. The latter study indeed evidence e.g. a significant and strong ( $R^2=0.8$ ) relationship between the FOTO index and stand total density (i.e. the finer is the canopy grain, the higher is the total tree density), while we obtained a non-significant opposite trend. This is not surprising because we calibrated the coarse-grain side of our gradient with mature climax evergreen stands (P, H) that contain a low tree density respectively to this forest type, and the fine-grain side with young semi-evergreen stands heavily degraded (K, J and to a lesser extent I) which also contain very few trees with respect to their own forest type (Ramseh et al., 2009). According to the typology of Ramseh and al (2009) and field observations, our study area is likely to contain semi-evergreen forests at its northern-west corner, close by the Uppagala village, whom should gradually change into evergreen ones toward the Southern-East corner, the latter type of forest having been further divided into climax and non-climax forests according to a floristic classification (Ramseh et al., 2009). Successional pathways from semi-evergreen to non-climax evergreen and further to climax evergreen have been evidenced with gradual changes in species composition and recruitment (increase in secondary and primary evergreen species, decrease in deciduous species) and also in structure. However, great structural variations within and between forest types, notably in terms of stem density, did not bring to light any predictable pattern with forest age. Chazdon et al. (2006) confirm the high variability of stem density within successional stages of Neo-tropical Costa-Rican secondary forests and underline the wide array of potential influencing factors (e.g. degradation intensity on the Ghats, Ramseh et al., 2009). If our study area would have encompass only one forest type (say climax evergreen), we would have certainly obtained the typical negative exponential trend of tree density as the undisturbed forest ages, but the cross-forest types characteristic of our model calibration prevent it. For FOTO to be properly **calibrated** on mixes of forest types, a forest structural parameter homogeneously evolving across forest types dynamics (i.e. not tree density) and consistently with canopy textural patterns (i.e. windows location on PCA axes) should be used. The mean tree diameter ( $D_g$ ), relating to basal area distribution and stem density, seems to capture this dynamic fairly well for rather homogeneous forests ( $R^2=0.7$ , Couteron et al., 2005) and mixed forest types ( $R^2=0.54$ ). Although Couteron (2005) do not find a significant relationship between FOTO index and stand basal area due to a lack of differences between sample plots values, this stand parameter significantly relate to our FOTO index ( $R^2=0.63$ ) and display an increasing trend as the canopy get coarser. Increasing evidences emphasize the good match of basal area with chronosequences trends, because it is more related to diameter and height growth rates of standing trees than net changes in tree density through recruitment and mortality (Chazdon et al., 2006). This metric may therefore be more conservative to calibrate FOTO performed over several forest types. Basal area is also known to be closely linked to AGB (Chazdon et al., 2006) and may be more representative of stand spatial attributes that are process-related (e.g. biomass accumulation) than other stand-level characteristics (e.g. age, height, density, etc.) which seems to correspond to the FOTO classification. For instance, the FOTO index reasonably ( $R^2=0.63$ ) and highly (up to  $R^2=0.91$ ) correlate with AGB estimates on our study area and the tropical mangrove forests of French Guiana (Proisy et al., 2007), respectively.

Lets finally note however that the most substantial patterns of vertical and horizontal spatial heterogeneity in tropical forest stands are often observed in the later stages of development (Frazer et al., 2005) which should drag mature climax evergreen stands on the coarsest side of PCA1 while less spatially heterogeneous though mature/dense semi-evergreen

stands may be less negatively ordinated along this axis. Yet, mature secondary tropical forests sometimes contain higher AGB or BA values than primary forests; a trend explained by the contribution of long-lived pioneers that disappear in the later stage (Chazdon *et al.*, 2006) and observed on the study area (Ramesh *et al.*, 2009). It follows that the first PCA axis alone should fail to linearly correlate with BA and one should retain and properly calibrate at least the 2 first axes.

#### ***4.3.3. Interest and remarks***

The method shown promising results for the characterization of the CWG wet tropical forests, which make worth investing in additional analyses and field sampling. A comparative analysis with smaller window sizes may rapidly lead to better results. Moreover, another field sampling seems necessary to complement the present one with more plot replicates per textural clusters, accurate the regression models and allow a model validation step. Nested sampling designs including forest types (or dominant species cohort) or window mean hillshade could also provide valuable insights for the development of the method. Yet, the current calibration of the FOTO model provide consistent trends with an increasing stand basal area throughout forest successional stages, from the degraded semi-evergreen secondary succession to the climax evergreen primary one. In their study of Cost-Rican tropical forest successions, Chazdon *et al.* (2010) underline an increase of basal area beyond 40 years after land abandonment (i.e. from exploited-land (e.g. pasture) to mature low-land wet forests), which offer good prospects to characterize forest “recovery” with FOTO if this relationship with BA hold after strengthening the model calibration. The effect of lighter land uses such as selective logging on forest structure have also been documented for the evergreen wet forests of the CWG; Ramesh *et al.* (2009) found a decrease from 39.3 m<sup>2</sup>.ha<sup>-1</sup> (un-logged stand) to 34.8 m<sup>2</sup>.ha<sup>-1</sup> (once selectively logged stand) which may be marked enough to be detectable by FOTO. Besides, selective logging usually target the largest trees in the stand which are often found in the canopy and particularly contribute to the patterns FOTO characterize, as shown by the higher match between structural parameters of trees greater than 30 cm dbh and the FOTO-derived textural indexes.

Lastly, although the FOTO model calibrated on the subset of largest trees per ground plots (i.e. > 30 cm dbh) display better fits than with a calibration on all measured trees (i.e. > 10 cm dbh), the differences of R<sup>2</sup> values are surprisingly small (e.g. R<sup>2</sup> of 0.79 to 0.54 for Dg, R<sup>2</sup> of 0.64 to 0.63 for BA) and very good fits are obtained with all measured trees in other studies (e.g. R<sup>2</sup> = 0.8 for tree density, Coutron *et al.*, 2005). This is particularly interesting because instinctively, one would think that FOTO being based on outer canopy textural patterns, it should provide structural information relative to the trees composing this top canopy layer (trees visible on the image) rather than to the entire stand population, while the good results obtain on the latter may indicate otherwise. Considering basal area or AGB for example, it seems logical that as the largest trees in a stand are often found in the canopy and account for the largest part of total stand AGB estimate, up-scaling our AGB model calibration from the “visible largest trees” (trees > 30cm dbh) to the “entire stand” (trees > 10 cm dbh) may only add some noise to the model fit related to variations in “non-visible” AGB across plots. A stake for the FOTO method would be to show that this relative proportion of “non-visible” AGB is constant across sites or, in other words, that there is an invariant scale factor between canopy trees’ AGB and sub-canopy trees’ or total stand AGB. As far as I know, the later relationship has not been demonstrated to day, but potential tracks arise from the metabolic theory of Enquist *et al.* (1998). This resource-based theory extends fundamental metabolic constraints operating at the individual level (animal & vegetal) to macro-ecological attributes observed at community level. Using a mechanistic model of biomass allocation, Enquist *et al.* (2001) demonstrate that the total number of trees (per dbh classes)

invariantly scale as -2 the power of mean Dg ( $Y \sim X^{-2}$ , Fig. 35) and -3/4 the power of standing AGB estimate, both within and across plant communities of varying geographic origins.

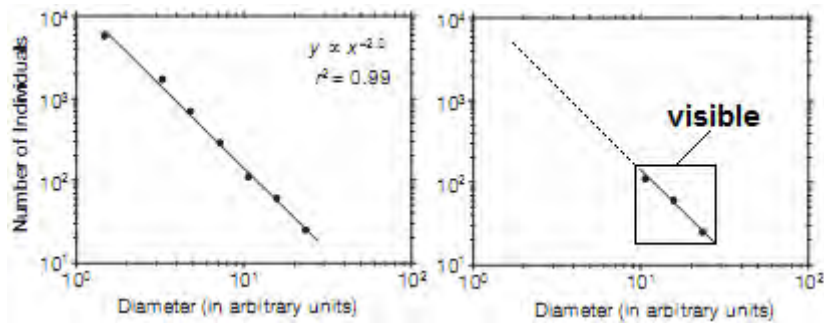


Figure 35. (left) Results of biomass allocation model simulations from Enquist and Nklas (2001); (right) regardless of their dbh (“arbitrary units”), the largest / canopy trees visible from the satellite image and characterized by FOTO may contain information relative to size-frequency distribution of all the trees within the stand.

Enquist *et al.* (2008) further state that in principle, it should be possible to extrapolate e.g. energy use or biomass of the entire stand from values of the largest trees, although their current model may lead to misleading predictions due to e.g. absence of density-independent mortality parameter. Developing and validating this theory would be a very important step for varying kind of remote sensing-based forest researches and particularly the FOTO method.

## Conclusions & Recommendations

Within the context of IFP research efforts to characterize and map Western Ghats tropical forests, we assessed the performances of the newly developed FOTO method and take advantage of this opportunity to focus on technical issues of particular interest with respect to the study site specificities (effect of topography variations) and socio-economical context (GE image quality). The latter difficulties / constraints being encountered worldwide, the present findings and discussion points are therefore not limited to the Indian context.

As performed in this project, the FOTO method provided a consistent characterization of forest canopy in spite of the marked topography variations and the structural complexity of the studied forests (high species diversity, high AGB range). We shown than topography variations only weakly influence the FOTO-derived textural index and that a simple technique, namely the partitioned standardization, coupled with a quickly computable hillshade model can tackle this influence. Other topographically induced effects such as the so called “local effect” did not induce major biases in the results and further investigations should allow correcting for this marginal drawback.

In term of forest structure inferring, we obtained good predictions on mean tree diameter ( $D_g$ ), stand basal area ( $G$ ) and AGB estimate, in agreement with ground plots particularities (distinct dynamics) and previous FOTO applications. Those promising results should be complemented by additional field samplings and improved by the use of smaller window size to limit the effect of spatial heterogeneity on window r-spectra computation, a textural component hindering the characterization of canopy patterns of interest. These steps are crucial to assess the performance of FOTO in characterizing forest stands located on the high side of the AGB range, an important stake for remote sensing-based tropical forest studies, but also to accurate the model calibration, achieve a validation step and compute prediction confidence intervals.

The interesting results obtained with GE images not only stress the potential value of this freely accessible satellite image database but also underline the operational asset of FOTO that provide consistent results with input images of different spatial resolutions and spectral content. We obtained reasonable correlations between forest structural parameters and GE-based FOTO index, although some extent of dissimilarities between IKONOS- and GE-derived results was highlighted pointing toward a need for further research. Nevertheless, it is apparent that GE-derived FOTO maps can be very useful to get a broad picture of tropical forest characteristics over thousand of unexplored area and it is not unrealistic to think that GE may serve as a spatially extensive – less detail data source in combination with high spatial resolution images to enable affordable landscape-level forest characterization.

## Bibliography

- Aiba S.I. and Kitayama K., 1999. Structure, composition and species diversity in an altitude-substrate matrix of rain forest tree communities on Mount Kinabalu, Borneo. *Plant Ecology*, vol. 140, n° 2, p. 139-157.
- Alparone L., Wald L., Chanussot J., Thomas C., Gamba P., Bruce L.M., 2007. Comparison of Pansharpening Algorithms: Outcome of the 2006 GRS-S Data-Fusion Contest. *IEEE Transaction on Geoscience and Remote Sensing*, vol. 45, n° 10, p. 3012-3021.
- Asner G.P., Palace, M. Keller, M. Pereira, R. J. Silva, J.N.M. & Zweede J.C. 2002. Estimating canopy structure in an Amazon forest from laser range finder and IKONOS satellite observations. *Biotropica*, n° 34, p. 483–492.
- Asner G.P. and Warner A.S., 2003. Canopy shadow in IKONOS satellite observations of tropical forests and savannas. *Remote Sensing of Environment*, n° 87, p. 521–533.
- Asner G.P., Knapp D.E., Balaji A. and Páez-Acosta G., 2009a. Automated mapping of tropical deforestation and forest degradation: CLASlite. *Journal of Applied Remote Sensing*, vol. 3, p. 1- 24.
- Asner G.P., Hughes R.F., Varga T.A., Knapp D.E. and Kennedy-Bowdoin T., 2009b. Environmental and Biotic Controls over Aboveground Biomass Throughout a Tropical Rain Forest. *Ecosystems*, n° 12, p. 261–278.
- Asner G.P., Hughes R.F., Varga T.A., Knapp D.E. and Kennedy-Bowdoin T., 2009c. Environmental and Biotic Controls over Aboveground Biomass throughout a Tropical Rain Forest. *Ecosystems*, vol. 12, p. 261–278.
- Baccini A., Friedl M.A., Woodcock C.E. and Warbington R., 2004. Forest biomass estimation over regional scales using multisource data. *Geophysical Research Letters*, vol. 31, L10501.
- Barbier N., Couteron P., Proisy C., Malhi Y., 2009. The variation of apparent crown size and canopy heterogeneity across lowland Amazonian forests. (in preparation for *Global Change Biology*)
- Bharati M.H., Liu J.J., MacGregor J.F., 2004. Image texture analysis: methods and comparisons. *Chemometrics and Intelligent Laboratory Systems*, vol. 72, p. 57– 71.
- Boyd D.S. and Danson F.M., 2005. Satellite remote sensing of forest resources: three decades of research development. *Progress in Physical Geography*, vol. 29, Issue 1, p. 1–26.
- Cha S., Park C., 2007. The utilization of Google Earth images as reference data for the multi-temporal land cover classification with MODIS data of North Korea. *Korean Journal of Remote Sensing*, vol. 23, p. 483-491.
- Chazdon, R.L., Letcher S.G., van Breugel M., Martinez-Ramos M., Bongers F., Finegan B., 2006. Rates of change in tree communities of secondary Neotropical forests following major disturbances. *The Royal Society* n° 362, p.273–289.
- Chazdon R.L., Finegan B., Capers R.S., Salgado-Negret B., Casanoves F., Boukili V., Norden N., 2010. Composition and Dynamics of Functional Groups of Trees During Tropical Forest Succession in Northeastern Costa Rica. *Biotropica*, vol. 42, Issues 1, p. 31– 40.
- CLASlite Haway REDD demo; CLASlite project, The Carnegie Institution for Science, available at <http://claslite.ciw.edu/en/support/documents.html>; visited the 01/06/2010.
- CLASlite Peru REDD demo; CLASlite project, The Carnegie Institution for Science, available at <http://claslite.ciw.edu/en/support/documents.html>; visited the 01/06/2010.
- Couteron P., 2002. Quantifying change in patterned semi-arid vegetation by Fourier analysis of digitised aerial photographs. *International Journal of Remote Sensing*, vol. 23, Issue 17, p. 3407-3425.

- Couteron P., Pélissier R., Mapaga D., Molino J.-F. & Teillier L., 2003. Drawing ecological insights from a management-oriented forest inventory in French Guiana. *Forest Ecology and Management*, vol. 172, p. 89–108.
- Couteron P., Pélissier R., Nicolini E. and Paget D., 2005. Predicting tropical forest stand structure parameters from Fourier transform of very high-resolution remotely sensed canopy images. *Journal of Applied Ecology*, vol. 42, p. 1121-1128.
- Couteron P., Barbier N. and Gautier D., 2006. Textural ordination based on Fourier spectral decomposition: a method to analyze and compare landscape patterns. *Landscape Ecology*, vol. 21, p. 555-567.
- De Jong S.M. and Van der Meer F., 2004. *Remote Sensing and Digital Image Processing*, vol. 5. Remote sensing image analysis - including the spatial domain. Utrecht.
- De Wasseige C. & Defourny P., 2002. Retrieval of tropical forest structure characteristics from bi-directional reflectance of SPOT images. *Remote Sensing of Environment*, vol. 83, p. 362–375
- Diggle P.J. 1990. *Time series. A biostatistical introduction.*, 4th edition. Oxford University Press, Oxford, UK.
- Eric S.K., John M.M. and Dobson M.C., 1997. The Use of Imaging Radars for ecological Applications (review). *Remote Sensing of Environment*, n°59, p141-156.
- Flavenot T., 2009. Biomass estimation for the wet tropical evergreen forests of the Western Ghats. AgroParisTech, Paris (France), MSc Thesis.
- Francois Husson, Julie Josse, Sebastien Le and Jeremy Mazet (2009). *FactoMineR: Factor Analysis and Data Mining with R*. R package version 1.12. <http://factominer.free.fr>, <http://www.agrocampus-ouest.fr/math/>
- Frazer G.W., Wulder M.A., Niemann K.O., 2005. Simulation and quantification of the fine-scale spatial pattern and heterogeneity of forest canopy structure: A lacunarity-based method designed for analysis of continuous canopy heights. *Forest Ecology and Management*, n° 214, p. 65–90.
- Fromard F., Vega C. and Proisy C., 2004. Half a century of dynamic coastal change affecting mangrove shorelines of French Guiana. A case study based on remote sensing data analyses and field surveys. *Marine Geology*, vol. 208, Issues 2-4, p. 265-280.
- Gastellu-Etchegorry J.P., Demarez V., Pinel V. and Zagolski F., 1996. Modeling radiative transfer in heterogeneous 3-D vegetation canopies. *Remote Sensing of Environment*, vol. 58, p. 131–156.
- Gastellu-Etchegorry J.P., Martin E., Gascon F., 2004. DART: a 3D model for simulating satellite images and studying surface radiation budget. *International Journal of Remote Sensing*, vol. 25, n° 1, p. 73–96.
- Gibbs H. K., Brown S., Niles J. O. and Foley J. A., 2007. Monitoring and estimating tropical forest carbon stocks: making REDD a reality. *Environmental Research Letter* 2: 1-13.
- Grace J., 2004. Understanding and managing the global carbon cycle. *Journal of Ecology*, vol. 92, p. 189-202.
- Greenberg J.A., Dobrowski S.Z. and Ustin S.L., 2005. Shadow allometry: Estimating tree structural parameters using hyperspatial image analysis. *Remote Sensing of Environment*, n° 97, p 15 – 25.
- Gu D. and Gillespie A., 1998. Topographic Normalization of Landsat TM Images of Forest Based on Subpixel Sun–Canopy–Sensor Geometry. *Remote Sensing of Environment*, n° 64, p. 166-175
- Hay G. J., Niemann K.O. and McLean G., 1996. An Object-Specific Image-Texture Analysis of H-Resolution Forest Imagery. *Remote Sensing of Environment*, vol. 55, p. 108-122.
- Hilker T., Coops N.C., Schwalm C.R., Jassal R.P.S., Black T.A., Krishnan P., 2008. Effects of mutual shading of tree crowns on prediction of photosynthetic light-use efficiency in a coastal Douglas-fir forest. *Tree Physiology*, vol. 28, p. 825–834.

- Houghton R.A., Lawrence K.T., Hackler J.L. and Brown S., 2001. The spatial distribution of forest biomass in the Brazilian Amazon: a comparison of estimates. *Global Change Biology*, vol. 7, p. 731–746.
- IFP Database, metadata of Uppangala permanent sample plot (UPSP). ID code: IFP-ECODATA-UPSP. Available at [www.ifpindia.org](http://www.ifpindia.org) (Biodiversity portal).
- Iverson L.R., Prasad A.M. and Rebeck J., 2004. A comparison of the integrated moisture index and the topographic wetness index as related to two years of soil moisture monitoring in Zaleski State Forest, Ohio. *Proceedings of the 14th Central Hardwoods Forest Conference GTR-NE-316*.
- Imhoff M. L., 1995. Radar backscatter and Biomass Saturation: Ramifications for Global Biomass Inventory. *IEEE Transactions on Geoscience and Remote Sensing*, vol. 33, p. 511-518.
- Kane V.R., Gillespie A.R., McGaughey R., Lutz J.A., Ceder K. and Franklin J.F., 2008. Interpretation and topographic compensation of conifer canopy self-shadowing. *Remote Sensing of Environment*, n° 112, p. 3820–3832.
- Kasischke E. S., Melack J. M., Dobson M. C., 1997. The use of imaging radars for ecological applications - a review. *Remote Sensing of Environment*, vol. 59, p. 141-156.
- Leboeuf A., Beaudoin A., Fournier R.A., Guindon L., Luther J.E., Lambert M.C., 2007. A shadow fraction method for mapping biomass of northern boreal black spruce forests using QuickBird imagery. *Remote Sensing of Environment*, n° 110, p. 488–500.
- Lee S. and Choi U., 2003. Development of GIS-based geological hazard information system and its application for landslide analysis in Korea. *Geosciences journal*, vol. 7, n°. 3, p. 243-252.
- Li X. and Strahler A. H., 1992. Geometric– optical bidirectional reflectance modeling of the discrete crown vegetation canopy: Effect of crown shape and mutual shadowing. *IEEE Transactions on Geoscience and Remote Sensing*, vol. 30, p. 276– 292.
- Lieberman D., Lieberman M., Peralta R. and Hartshorn G.S., 1996. Tropical Forest Structure and Composition on a Large-Scale Altitudinal Gradient in Costa Rica. *Journal of Ecology*, vol. 84, n° 2, p. 137-152.
- Lu D., 2006. The potential and challenge of remote sensing-based biomass estimation. *International Journal of Remote Sensing*, vol. 27, n°. 7, p. 1297–1328 .
- Lucas R. M., Mitchell A. L., Rosenqvist A., Proisy C., Melius A. and Ticehurst C., 2007. The potential of L-band SAR for quantifying mangrove characteristics and change: case studies from the tropics. *Aquatic Conservation: Marine and Freshwater Ecosystems*, vol. 17, p. 245-264.
- Lu D., Mausel P. Brondizio E. & Moran E., 2004. Relationships between forest stand parameters and Landsat TM spectral responses in the Brazilian Amazon Basin. *Forest Ecology and Management*, vol. 198, p. 149–167.
- Malhi Y. and Román-Cuesta R.M., 2008. Analysis of lacunarity and scales of spatial homogeneity in IKONOS images of Amazonian tropical forest canopies. *Remote Sensing of Environment*, vol. 112, n° 5, p. 2074–2087.
- Madelaine-Antin C., 2009. Dynamique des peuplements forestiers tropicaux hétérogènes: variabilité inter et intraspécifique de la croissance des arbres et trajectoires de développement en forêt dense humide sempervirente, dans les Ghâts occidentaux de l’Inde. Université Montpellier 2, Montpellier (France), PhD Thesis.
- Minang P.A. and Murphy D., 2010. REED Après Copenhague : La Voie À Suivre. International Institute for Sustainable Development (IISD).
- Miyajima Y., Takahashi K., 2007. Changes with altitude of stand structure of temperate forests on Mount Norikura, central Japan. *Journal of Forest Research*, vol. 12, n° 3, p. 187-192.

- Montesano P.M., Nelson R., Sun G., Margolis H., Kerber A. and Ranson K.J., 2009. MODIS tree cover validation for the circumpolar taiga–tundra transition zone. *Remote Sensing of Environment*, vol. 113, p. 2130-2141.
- Mugglestone M.A., & Renshaw E., 1998. Detection of geological lineations on aerial photographs using two-dimensional spectral analysis. *Computers and Geosciences*, vol. 24, 771-784.
- Mumby P.J., and Edwards A.J., 2002. Mapping marine environments with IKONOS imagery: Enhanced spatial resolution can deliver greater thematic accuracy. *Remote sensing of Environment*, vol. 82, p. 248-257.
- Myers N., 1990. The biodiversity challenge: expanded hot-spot- analysis. *The Environmentalist*, vol. 10, Issue 4, p. 243-256.
- Noguchi M. and Yoshida T., 2005. Factors influencing the distribution of two co-occurring dwarf bamboo species (*Sasa kurilensis* and *S. senanensis*) in a conifer-broadleaved mixed stand in northern Hokkaido. *Ecological Research*, vol. 20, p. 25-30.
- Oladi D., 2001. Developing a forest growth monitoring model using Thematic Mapper imagery. *Proceedings of the 22<sup>nd</sup> Asian Conference on Remote Sensing*, 05–09 November, Singapore.
- Pascal J.P. and Pélissier R., 1996. Structure and floristic composition of a tropical rain forest in southwest India. *Journal of Tropical Ecology*, vol. 12, p. 195–218.
- Pélissier R., 1995. Relations entre l'hétérogénéité spatiale et la dynamique de renouvellement d'une forêt dense humide sempervirente : forêt d'Uppangala, Ghâts occidentaux de l'Inde. Université Claude Bernard, Lyon (France), PhD Thesis.
- Pélissier, R. 1997. Hétérogénéité spatiale et dynamique d'une forêt dense humide dans les Ghats occidentaux de l'Inde. Institut français de Pondichéry, Inde, Publications du département d'écologie, vol. 37, p. 1-148.
- Pélissier, R. 1998. Tree spatial patterns in three contrasting plots of a southern Indian tropical moist evergreen forest. *Journal of Tropical Ecology*, vol. 14, n° 1, p. 1-16.
- Peucker T.K., Fowler R.J., Little J.J., 1978. The Triangulated Irregular Network. *Proceedings of the ASP-ACSM Symposium on DTM's*. St. Louis, Missouri, October 1978.
- Potere D., 2008. Horizontal Positional Accuracy of Google Earth's High-Resolution Imagery Archive. *Sensors*, vol. 8, p. 7973-7981.
- Proisy C., Coueron P. and Fromard F., 2007. Predicting and mapping mangrove biomass from canopy grain analysis using Fourier-based textural ordination of IKONOS images. *Remote Sensing of Environment*, vol. 109, Issue 3, p. 379-392.
- Ramankutty N., Gibbs H. K., Achard F., Defriess R., Foley J. A. and Houghton R. A. 2007. Challenges to estimating carbon emissions from tropical deforestation. *Global Change Biology*, vol. 13, p. 51-66.
- Ramesh, B.R., Swaminath, M.H., Patil S., Aravajy S., Elouard C., 2009. Assessment and conservation of forest biodiversity in the Western Ghats of Karnataka, India. 2. Assessment of tree biodiversity, logging impact and general discussion. *Pondy Papers in Ecology*, n°7. Institut Français de Pondichéry.
- Read J.M., Clark D.B., Venticinque E.M. & Moreiras M.P., 2003. Application of merged 1-m and 4-m resolution satellite data to research and management in tropical forests. *Journal of Applied Ecology*, vol. 40, p. 592-600.
- Renshaw E. and Ford E. D., 1984. The description of spatial pattern using two-dimensional spectral analysis. *Vegetation*, vol. 56, p. 75–85.
- Ripley B.D., 1981. *Spatial Statistics*. Wiley, New York, NY.
- Soenen S.A., Peddle D.R. and Coburn C.A., 2005. *IEEE Transaction on Geoscience and Remote Sensing*, vol. 43, n° 9, p. 2148-2159.
- Thompson I., Mackey B., McNulty S., Mosseler A., 2009. Forest Resilience, Biodiversity, and Climate Change. A synthesis of the biodiversity/resilience/stability relationship in forest

- ecosystems. Secretariat of the Convention on Biological Diversity, Montreal. Technical Series n° 43, 67 pages.
- Tuomisto H., Ruokolainen K., Kalliola R., Linna A., Danjoy W. & Rodriguez Z., 1995. Dissecting Amazonian biodiversity. *Science*, vol. 269, p. 63–66
  - Van Den Eeckhaut M., Poesen J., Verstraeten G., Vanacker V., Moeyersons J., Nyssen J. and van Beek L.P.H., 2005. The effectiveness of hillshade maps and expert knowledge in mapping old deep-seated landslides. *Geomorphology*, vol. 67, Issues 3-4, p. 351-363.
  - Wang X., Fang J., Tang Z., Zhu B., 2006. Climatic control of primary forest structure and DBH–height allometry in Northeast China. *Forest Ecology and Management*, vol. 234, p. 264-274.
  - Wulder M. A., Le Drew E. F., Franklin S. E. & Lavigne M., 1998. Aerial image texture information in the estimation of northern deciduous and mixed wood forest leaf area index (LAI). *Remote Sensing of Environment*, vol. 64, p. 64-76.

## **Acknowledgements**

I am deeply indebted to Dr. R. Pélissier for the considerable time he invested in this project as well as Dr. C. Proisy for his help and support in implementing the FOTO method. I would also like to warmly thank the field team for the hard work carried out in the Western Ghats wet forests, namely Q. Renard, S. Ramalingam, T. Gopal, Adimoolam K. and the Obbaya's family. I am also grateful to Dr. N. Ayyappan and Dr. K. Narendran for the good time spent in the Ecology department of the IFP. Finally, I would like to thank my supervisors from Wageningen University, J. den Ouden and J. Clevers, for their valuable feedbacks and comments.

1. CLAIRE ELOUARD, FRANÇOIS HOULLIER, JEAN-PIERRE PASCAL, RAPHAEL PÉLISSIER, B.R. RAMESH. Dynamics of the dense moist evergreen forests. Long Term Monitoring of an Experimental Station in Kodagu District (Karnataka, India), 1997, n°1, 23 p.  
<http://hal.archives-ouvertes.fr/hal-00373536/fr/>
2. FRANÇOIS HOULLIER, YVES CARAGLIO, MURIEL DURAND. Modelling Tree Architecture and Forest Dynamics. A Research Project in the dense moist evergreen forests of the Western Ghats (South India), 1997, n°2, 37 p.  
<http://hal.archives-ouvertes.fr/hal-00373538/fr/>
3. MURIEL DURAND. Architecture and growth strategy of two evergreen species of the Western Ghats (South India), *Knema attenuata* (J. Hk. & Thw.) Warb. (Myristicaceae) and *Vateria indica* L. (Dipterocarpaceae) 1997, n° 3, 39 p.  
<http://hal.archives-ouvertes.fr/hal-00373540/fr/>
4. FRANÇOIS HOULLIER, RANI M. KRISHNAN, CLAIRE ELOUARD. Assessment of Forest Biological Diversity. A FAO training course. 1. Lecture Notes 1998, n° 4, 102 p.  
<http://hal.archives-ouvertes.fr/hal-00373545/fr/>
5. CLAIRE ELOUARD, RANI M. KRISHNAN. Assessment of Forest Biological Diversity. A FAO training course. 2. Case study in India, 1999, n° 5, 75 p.  
<http://hal.archives-ouvertes.fr/hal-00373548/fr/>
6. B. R. RAMESH, MOHAN SEETHARAM, M. C. GUERO, R. MICHON. Assessment and Conservation of Forest Biodiversity in the Western Ghats of Karnataka, India. 1. General Introduction and Forest Land Cover and Land Use Changes (1977-1997), 2009, n° 6, pp. 1-64.  
<http://hal.archives-ouvertes.fr/hal-00408263/fr/>
7. B. R. RAMESH, M. H. SWAMINATH, SANTHOSHAGOUDA PATIL, S. ARAVAJY, CLAIRE ELOUARD. Assessment and Conservation of Forest Biodiversity in the Western Ghats of Karnataka, India. 2. Assessment of Tree Biodiversity, Logging Impact and General Discussion. 2009, n° 7, pp. 65-121.  
<http://hal.archives-ouvertes.fr/hal-00408305/fr/>
8. QUENTIN RENARD, G. MUTHUSANKAR, RAPHAEL PÉLISSIER. Data Paper: High-resolution topographical and bioclimatic data for the Southern Western Ghats of India (IFP\_ECODATA\_BIOCLIM). 2009, n° 8, 21p.  
<http://hal.archives-ouvertes.fr/hal-00411120/fr/>
9. QUENTIN RENARD, B. R. RAMESH, G. MUTHUSANKAR, RAPHAEL PÉLISSIER Data Paper: High resolution vegetation cover data for the Southern Western Ghats of India (IFP\_ECODATA\_VEGETATION). 2010, n° 9, 12p.  
<http://hal.archives-ouvertes.fr/hal-00481614/fr/>
10. PIERRE PLOTON Analyzing canopy heterogeneity of the tropical forests by texture analysis of very high resolution images – a case study in the Western Ghats of India. 2010, n° 10, 64p